2009

California State University Northridge

CSUN Pedalsports
Human Powered Vehicle Project

[FINAL DESIGN REPORT]

The University Corporation
Research, Investments, and Commercial Services

AIRTECH

INDUSTRIAL METAL SUPPLY COMPANY
SINCE 1948

GENTLE GIANT
STUDIOS

CYCLE WORLD

SolidWorks

Associated Students

ASME
SETTING THE STANDARD

Abstract

This is the fourth year California State University Northridge (CSUN) has participated in ASME's Human Powered Vehicle Challenge. Last year, the CSUN Pedalsports team designed an elongated three wheeled design, with an innovative limited slip two-wheel drive system. This year, CSUN's design team has embarked on a new, fully composite two wheeled human powered vehicle. Using a clean sheet design, CSUN Pedalsports has incorporated its extensive experience in cycling to develop a new take on a slender semi-upright, ergonomic HPV. The vehicle is designed specifically for the ASME HPV Challenge, to be a marketable solution for sprints, endurance, as well as commuting.

The Human Powered Vehicle Association defines a human powered vehicle as "any kind of transportation powered by its human rider[s]." Whether by air, land, or water, these types of vehicles will always be popular, as they are a simple and efficient means of transportation. With the onset of increasing energy costs, diminished resources, and a heightened global awareness, the demand for human powered vehicles will only continue to rise. For this reason, the CSUN Pedalsports team is eager to develop a new HPV that pushes the envelope in versatility. We have strived to develop an extremely efficient, maneuverable and marketable solution to human powered ground transportation. After numerous iterations, the 2009 CSUN Pedalsports team is pleased to announce that it has designed such a vehicle, the P.F.C.S.U.2.W.H.P.G.V. or "Partially Faired Composite Semi-Upright 2 Wheeled Human Powered Ground Vehicle." This vehicle design has been optimized for use in the ASME HPVC.

Utilization of modern data acquisition tools in conjunction with engineering analysis allowed the CSUN Pedalsports team to accomplish this goal. The development testing was accomplished using a bike fit apparatus, Cyber Scanning, motion capture, human power measurement devices (Powertap), vibration meters, and tensile test machines. The initial data acquired was then applied to the ergonomic design and analysis of the vehicle. Using finite element analysis (FEA), computational fluid dynamics (CFD), and physical testing, the design went through many stages of optimization through this iterative process. The final design will be verified through physical testing including additional power testing, tuft testing, and if time permits, wind tunnel verification. Each process is discussed in more detail throughout this design report.

Design Description

The 2009 CSUN Pedalsports team consists of lead engineers who are experienced members from last year's team; several are avid cyclists and now graduating seniors. Last year, CSUN placed 6th overall, more than doubling our placement from prior years, but there is still room for improvement. We believe that the riders could perform even better if the vehicle was optimized around the rider's position. Last year's competition was also a place for this year's lead engineers to take note on possible design alternatives. A very valuable lesson learned from last year was to keep rider training time and ergonomics into account.

The preliminary concepts that were considered for this year's human powered vehicle were designs consisting of both two wheeled and three wheeled configurations in various riding positions. Five positions were considered prior to the determination of the final concept: recumbent, semi-recumbent, prone, semi-upright, and upright. The overall design matrix for each riding position in a faired and unfaired vehicle is shown in Table 1.

Table 1. Overall Design Matrix

HPV Overall Design Matrix									
	Un-faired				Faired				
Design Criteria	Recumbent	Semi-Recumbent	Upright	Semi-Upright	Recumbent	Semi-Recumbent	Upright	Semi-Upright	Weight
Aerodynamics	2.5	2	0	2	5	4	3	4	20.00%
Weight	3	3	4	5	2	2	3	4	10.00%
Manufacturability	2	2	4	4	1	1	3	3	5.00%
Safety	1	2	3	3	2	4	4	4	20.00%
Stability (Rideability)	2	3	5	4	1	2	4	3	15.00%
Acceleration	2	2	3	4	3	3	4	5	10.00%
Training Time	2	3	5	5	1	2	5	5	15.00%
Rider Comfort	2	4	4	2	1	3	5	4	5.00%
Totals	1.8	2.3	2.9	3.15	2	2.6	3.45	**3.55**	100.00%

Each position is ranked according to a few key design criteria. These criteria are weighed relative to their importance in vehicle performance, and are shown in the right most column. It can be seen that aerodynamics was judged to be the most important factor to consider in designing a human powered vehicle, and determining the optimal riding position. A rank value between 1 and 5 is given to each position in response to these criteria. After summing all the values assigned for each riding position, the faired semi-upright position was determined to be the optimal riding position.

The advantages of the semi upright riding position over the others are that it allows for more efficient acceleration and better stability and handling in corners. Since the upright riding position is the most common found on the majority of bicycles, most people have experience and are comfortable riding in this semi-upright position. Another major advantage of choosing this position is that because it is common, the muscles used to power the vehicle won't need any new training.

For this reason, the CSUN Pedalsports team has decided upon a new design for 2009. This design is built around the selected rider's comfortable cycling geometry, thus allowing them to train the proper muscle groups on their own road bicycles, and eliminating "the wait to train." Another observation, made from previous recumbent designs, was that muscle groups are isolated in such a configuration. This isolation prevented riders from recovering energy, as they could not alternate muscle groups by changing position. Nor could they vary muscle groups to cater to handling, accelerating, or sprinting.

In order to have the best design for the ASME HPVC, it is necessary to have a vehicle capable of fast straight-line speed, with the ability to maintain nimble handling characteristics as well as quick acceleration out of lower speed areas. With this in mind, it is important to stress the importance of human ergonomics, maximizing the efficiency and power of the rider. This is especially important when the 4+ riders will be spending most of their time designing, analyzing, and manufacturing the vehicle. As a result, there will be a limited time to actually train on the designed vehicle.

The 2009 CSUN Pedalsports P.F.C.S.U.2.W.H.P.G.V will offer improvements to other designs in many areas: as mentioned before, in the area of rider readiness, human power utilization, and versatility. Also, this design will integrate the rider as part of the fairing, allowing the rider to utilize a faired position when aerodynamics is the leading factor to maximize speed or efficiency. When a more powerful upright position is ideal, for acceleration or handling at lower speeds, the rider will not be hindered by an enclosure. This, of course, yielded some intricate design challenges that the team has overcome.

The primary design challenge was to utilize the rider as a means of power AND aerodynamics, thus eliminating the need for redundant fairing material. The most complex portion of this challenge was engineering a fairing. This fairing seamlessly connects the bike to the rider allowing for free rider movement, and maintaining smooth air flow while in the tucked position. This was a significant challenge, and required many hours of testing and analysis. The most important step was to properly analyze the rider's position while pedaling, to ensure proper design before manufacturing the prototype components.

Engineering all the components of any vehicle would take an extremely long period of time, and for many components it would be akin to "reinventing the wheel". All of the hardware, including the wheels, handlebars, seat tube, fork, and wheels will be commercially available 700c road bike components. The net effect of using these commercially available parts is twofold: commercial parts are easily obtained and interchangeable, and using standard parts allows more time to be put toward engineering the largest key systems and components, namely the frame, and fairing pieces.

Ergonomics

It is important to have the final frame design to be biomechanically efficient, allow for aerodynamic positions, and to be relatively comfortable. In order to transfer power efficiently, a bicycle frame would have to be built specifically for an individual. However, since there will be five different riders each with their own unique physical measurement, the frame had to be designed to accommodate everyone. A fit bike was used to obtain each rider's measurements in their optimal position which can be seen in Figure 1 below. The critical dimensions of the frame were the handlebar height (from the ground), stem length, virtual top tube length, and seat tube angle. All other key dimensions, such as crank length, handlebar width, and seat height were decided upon through averaging the dimensions from the riders' current preferences.

Figure 1. Fit Bike Used to Obtain Frame Geometries for Each Rider.

During the endurance event, the vehicle exchange is a critical period. The time taken to change vehicle geometries to accommodate different riders can consume precious time. In order to create the smoothest transition possible, it was decided to make all the adjustments via replaceable preset seat mast assemblies. The handlebar position will be fixed during the competition; therefore, the final geometry was designed to accommodate every rider. To do this, both the handlebar height and stem length dimensions were averaged. The final averaged dimensions were then locked down on the fit bike, and used as a template. The template was recorded through scaled profile pictures and cyber scanning. These templates were used for both frame and fairing design, as well as aerodynamic analysis. The final frame geometry, with the averaged positions can be seen in the SolidWorks model below.

Figure 2. Solidworks Model of Frame with Final Dimensions.

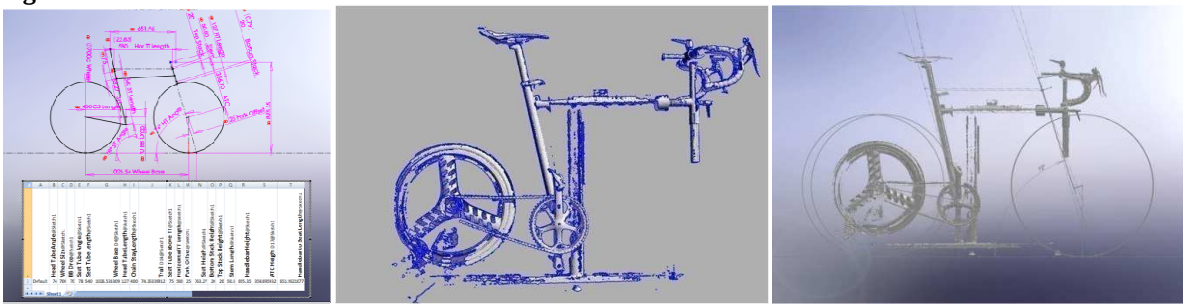

Once the fit bike was set to the final dimensions, it was used to obtain front, side, and top profile pictures in the hoods, drops, and aero positions for each rider. This was done by having the riders get into each of the positions mentioned above with their seat height set to the appropriate dimension. Once in the position, a picture was taken from all three directions. A side profile picture of one of the riders can be seen below in Figure 3. These pictures were used to plot a preliminary profile which was then be used for preliminary aerodynamic analysis. Later, these profile pictures were replaced with cyber scanning of the riders in the identical positions.

Figure 3. Side Profile of One Rider on Fit Bike with Final Dimensions.

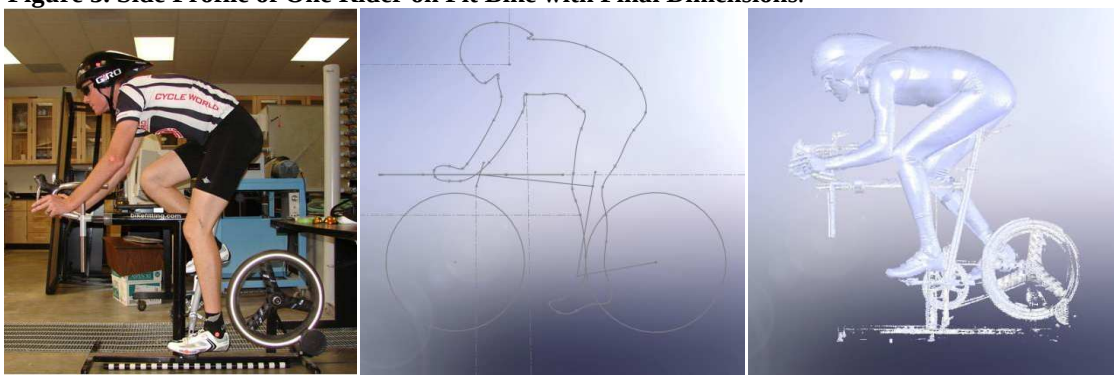

Body scanning was conducted for each male rider and one of the female riders on the fit bike. The fit bike was set in the averaged geometry, and each rider's individual seat positions were adjusted. The scanning heavily assisted the final design of the frame and fairing. The individual rider scans were used to visualize the riders in three dimensions within SolidWorks, and enabled the designers to create the frame and fairing accurately around the riders with proper ergonomics, and safety in mind. The scan of one rider on the fit bike position, integrated for frame design ,can be seen in Figure 4.

Figure 4. Body Scan of Rider by Gentle Giants Studios

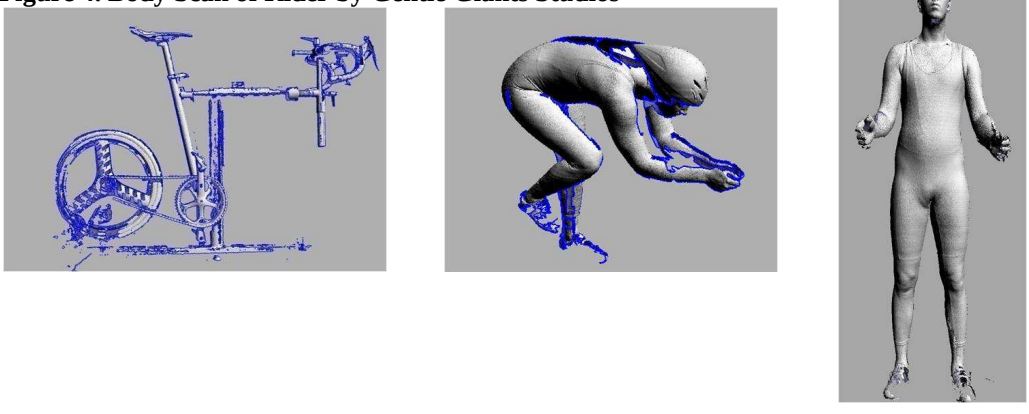

Frame Features and Design Innovations

With the rider geometry locked down, the frame design took shape. The structural design concept of this vehicle was largely inspired by carbon monocoque track, and time trial bicycles. These vehicles had both positive and negative traits. The most valuable trait of the time trial bike was the aerodynamic shape, unfortunately these frames were known to be difficult to size, and lacked the torsional and lateral stiffness of a contemporary, less aerodynamic high end frame. By contemporizing the structure of the design, incorporating geometry adjustments, and optimizing a fairing to conform perfectly to this already aerodynamic concept, the team was confident a versatile vehicle could be made for speed, endurance and the daily grind.

Figure 5. P.F.C.S.U.2.W.H.P.G.V V86 - Final Frame Design, Without Fairing.

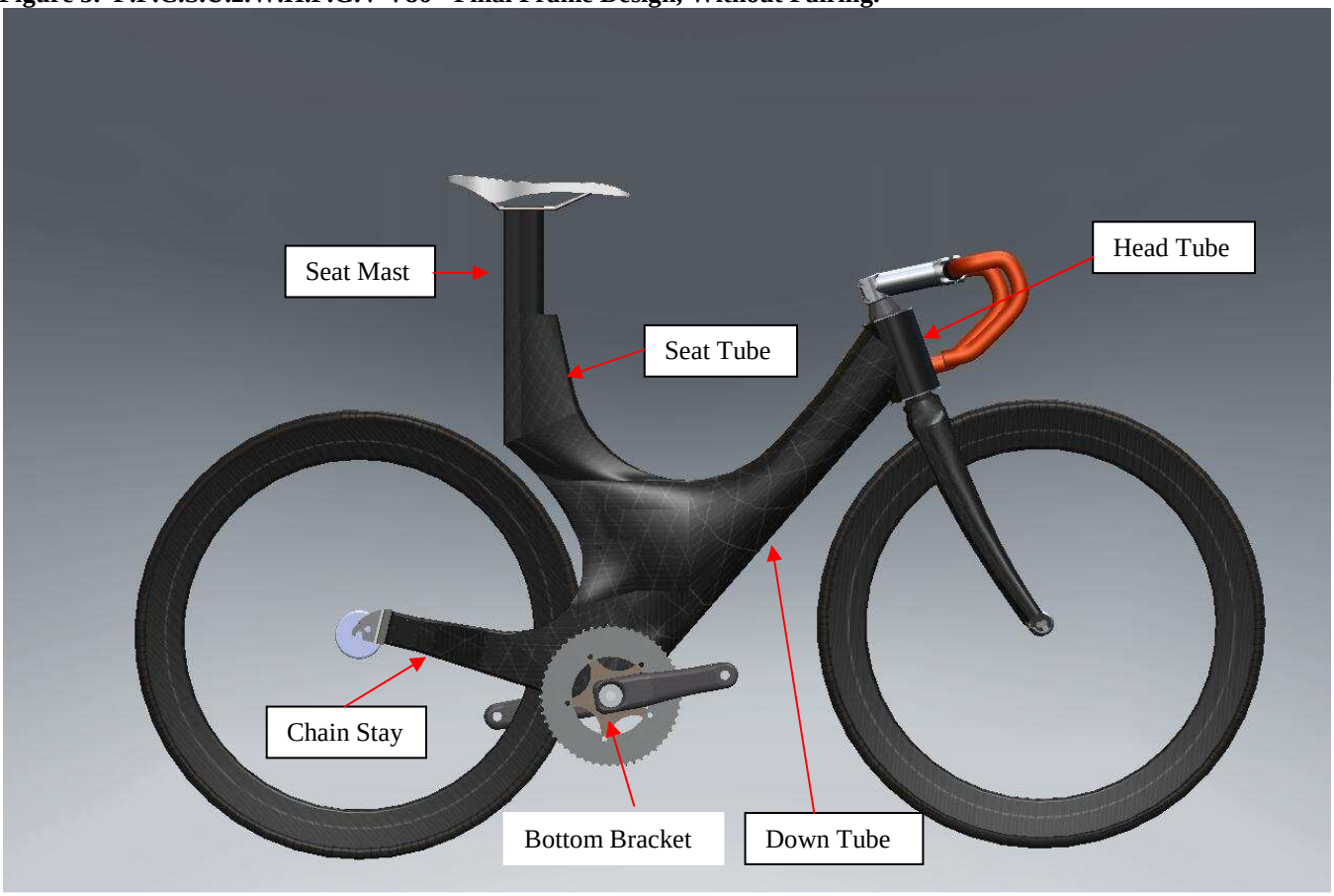

The final vehicle concept, P.F.C.S.U.2.W.H.P.G.V. V86, allowed the team to have an aerodynamic, one piece frame design that utilizes the tensile properties of carbon fibers to seamlessly "connect the dots" between the core structural areas. The frame shape was envisioned from drawing lines from the head tube, which supports the front wheel and the rider's upper body, to the bottom bracket, supporting the riders pedal inputs and lower body weight, directly to the rear wheel. This design was specifically intended for carbon, taking full advantages of its tensile properties. Many additional design features were added to the final design and will be discussed below.

The V86's large diameter, tear drop shaped tubes and monocoque center section were designed to add torsional and lateral stiffness in the head tube and bottom bracket regions. The tube diameters are approximately 1.5x that of the stiffest road frames on the market. This conservative tube design ensures a safe design that is structurally sound for the first iteration. Further optimization is planned for next year's design by modifying the tear drop tube shapes (Figure 6) to true airfoil cross sections.

The frame was made even stronger by using low density "pink foam," which added stiffness as well as a permanent structure to wrap the carbon around. Another benefit to using this foam was that it acted as structure to guide internal cable routing. This internal routing keeps the frame clean and hides the shifter and brake cables from airflow.

At the same time, the designs low slung shape allows for mounting and dismounting clearance for a wide range of riders (Figure 5). This also meant that the design would accommodate the team's smaller female riders, and in the case of production, would require less size runs. The team's prototype of the P.F.C.S.U.2.W.H.P.G.V. V86, would be considered the

larger of the two models. V86 allows all of our riders, who range from 5'7" to 6'4", to fit comfortably with just the exchange of a seat mast. The seat mast, acquired from a 2009 Specialized Transition, accomplished this through the use of different setbacks. Setbacks allow the frame to have an adjustable top tube and seat angle range.

The low slung design feature was also carried through to the bottom bracket. The bottom bracket drop of CSUN's vehicle is about 90mm below the axle of its 700c wheels. This equates to a bottom bracket height of ten inches. The net effect of this adjustment recesses the rider into the frame creating less frontal area, and accommodates a sleeker fairing.

Figure6. Cross Section of Tube Shape

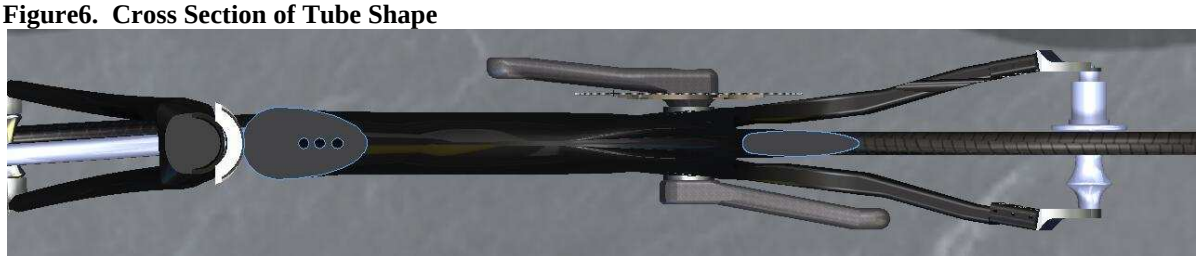

Figure 7. Cross Section Illustrating Pink Foam Core and Internal Cable Routing

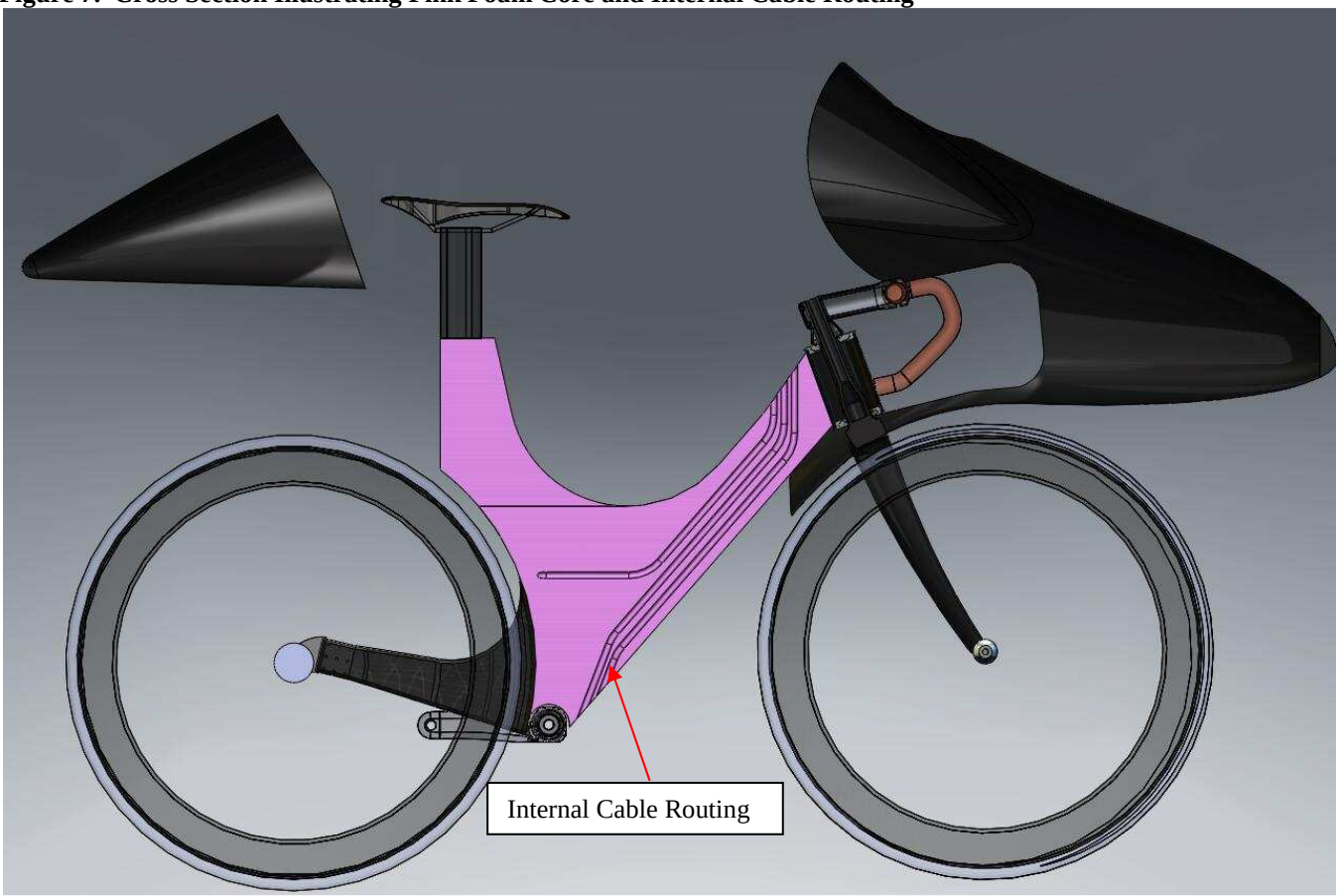

A new industry standard for bottom brackets has been set forth by Cannondale Bicycles. A larger bottom bracket shell, dubbed BB30, offers clearance for stiffer and lighter cranks spindles. This feature has three advantages: increased lateral stiffness, by eliminating deflection in the crank arms, no thread interface for simple slip fit bearing installment, and adaptability to older standards if desired. The BB30 was chosen for the P.F.C.S.U.2.W.H.P.G.V. to increase strength, reduce flex during cycling, reduced weight, increased stiffness during operation, ease of manufacturing, as well as keeping current with industry standard.

Figure 8 shows the most innovative feature integrated into the vehicle: an adjustable head tube assembly. This feature allows the team to customize the rake angle of the steering system based on course conditions. The rake angle has settings of 68, 70, and 72 degrees. The slack, 68 degree setting is designed for stability at high speeds, such as the sprint course. But when nimble handling is desired for the tight corners of the endurance course, the head tube can be accurately adjusted to the steep (72') setting. This is accomplished via two keyed aluminum eccentric cups which are offset along a 2 degree axis. The keys keep the offset cups aligned accurately, and without binding. The cup sets were also designed to be

adaptable for any commercially available fork's steerer tube size. Any combination between 1" and 1.5" steerer tubes may be used with this system, and will still allow for the full 6 degree range of adjustment.

Figure8. Eccentric Head Tube Assembly 6 Degrees of Accurate Angle Adjustment

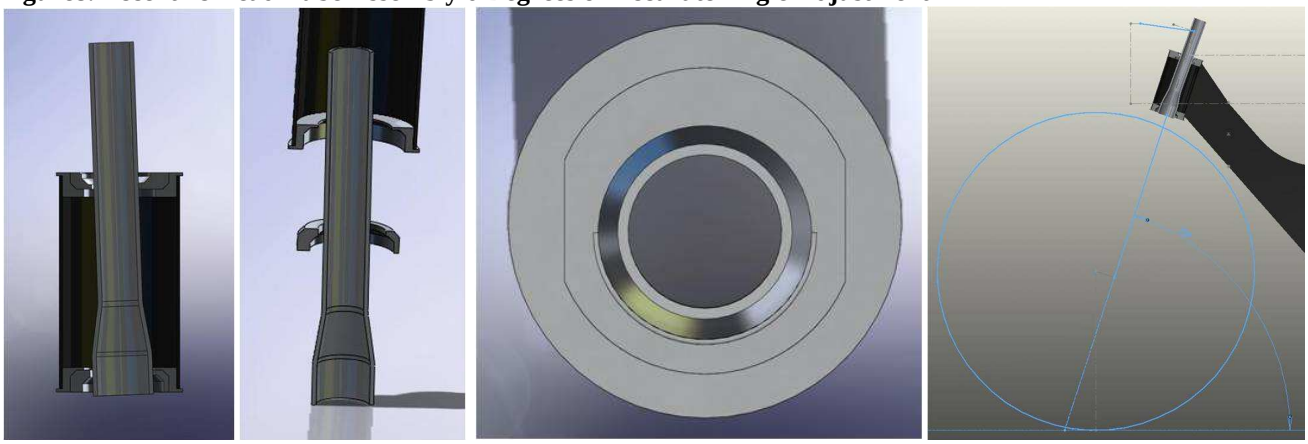

Aerodynamics

Aerodynamic drag is by far the largest resistive force on human powered vehicles traveling above 10 mph. In fact, at 22 mph the aerodynamic drag constitutes approximately 86% of the total resistive force exerted on the vehicle. For this reason the aerodynamics of the HPV are of the utmost importance.

In order to improve the aerodynamics of the HPV special care was taken to optimize the aerodynamics of both the rider and the vehicle. Since the rider accounts for approximately 80% of the total aerodynamic drag [4] front and rear fairings are employed. Both fairings were designed primarily to direct the flow over and around the rider, thus largely reducing the total drag. To achieve this, approximately 50% of the frontal cross-sectional area of the vehicle and rider is covered by the front fairing. Despite the streamlining at the front of the vehicle, a large amount of drag still exists. This drag exists as pressure drag and occurs behind the riders back and posterior as flow separation creates large turbulent vortices. These turbulent vortices create a suction or pressure drag behind the rider. To combat this phenomenon the design employs a rear tail cone fairing. The rear fairing is designed to slowly reintroduce the disturbed air into the free stream and prevent the abrupt transition from rider to empty space.

In an attempt to further streamline the rider, off-the-shelf aerodynamic helmets will be used by all riders in all phases of the competition, aerodynamic helmets reduce pressure drag behind the riders head and help to direct the air smoothly down the riders back.

The wheels of the vehicle are yet another source of drag. For this reason aerodynamic wheels will be used in both the front and rear for all competitions. Deep section carbon rims and spoked wheels were chosen for the front as they possess excellent drag characteristics while limiting susceptibility to large side forces. Because the front wheel is used to steer the vehicle, side forces resulting from yaw angles or wind gusts are of prime concern. Deep section carbon rims with spoked wheels have a low side force coefficient for yaw angles between 0 and 90 degrees, relative to other aerodynamic wheel options. The aforementioned design also possesses excellent drag coefficient characteristics over large yaw angles and wheel speed ranges with consistent and predictable values. A solid carbon disc wheel is the ideal wheel for the rear of vehicle for its exceptional drag coefficient characteristics. Since the rear wheel sees limited yaw angles and is not responsible for steering, side forces are less critical. Solid carbon disc wheels have the lowest drag coefficient of all aerodynamic wheels for yaw angles near zero. However, the drag coefficient at low wheel speeds (below 10 mph) and around 6 to 8 degrees of yaw sharply increases due to flow separation. This effect is drastically attenuated at higher wheels speeds and is therefore not a hindrance to performance. Due to the nature of the large solid surface area created by the carbon disc wheel the side force coefficient can be extremely large. At yaw angles of 90 degrees the solid carbon disc wheel had the highest side force coefficient of any aerodynamic wheel tested. As mention earlier, at around 6 to 8 degrees of yaw angle and low wheel speeds (below 10 mph) flow separation occurs. However, in this case, the flow separation drastically reduces the side force coefficient. For this reason, side forces during low speed corners should not be an issue. The increased surface area of both front and rear wheels makes them more susceptible to wind gust .Therefore a deep section carbon rimed front wheel and solid carbon disc rear wheel would be used during favorable weather conditions only [5].

Based on aerodynamics and cost considerations, our design will employ Easton EC 90 Aero wheels in both the front and rear. The EC 90 aero wheel is a traditional spoked wheel with deep section carbon rims. Unfortunately, due to budget constraints, a full carbon disc rear wheel will not be used on the rear of the vehicle.

Figure 9. Solid Works Model of Frame Fairing and Rider.

Material Selection and Manufacturing Process

The ideal material for HPV construction should have low weight and high strength. Specific properties of interest are density, elastic modulus, Poisson's ratio, and tensile strength. For a given set of design constraints, there will be an optimal material for each component.

Previous CSUN designs proved to be robust but heavy relative to the competition. Having such a large mass made it very difficult to accelerate out of corners during the endurance course, and it lengthened the necessary runway for our vehicle to achieve its top speed during the sprint course. The 2008 HPV weight was in the range of one hundred pounds, whereas the top competitors were approximately forty to fifty pounds. Therefore, vehicle weight reduction was a heavily weighted design consideration.

Previous frames produced for the HPV project have been manufactured mostly using aluminum tubing. Last year's frame, besides being heavy, was not sufficiently stiff. The frame allowed for too much deflection during intense rider input to the cranks, as well as in corners. This was caused by the torsional deflection, of the main spar, as it was poorly braced and overly long. Thus the efficiency of the vehicle was compromised by the frames lack of rigidity. This observation informed the materials research performed by this year's team.

Table 2 provides a summary of the properties for candidate materials. Compared to steel, aluminum has the same specific modulus, while also having a density of just over one third. Thus, potentially a frame built out of aluminum could be stiffer and lighter than a frame built of steel. Titanium could also be a great choice for frame material. Titanium has the same specific modulus as aluminum and steel, while also having a tensile strength nearly as high as steel. It is possible to produce a very lightweight and stiff frame using titanium, though there are still other viable materials to consider.

Table 2 shows the properties for several composite materials, which offer significant advantages over metals. For example, carbon fiber displays a density lower than that of aluminum with a specific tensile strength five times that of steel and specific modulus over 6 times larger than steel, titanium, and aluminum. Another advantage is that composites typically have stress or fatigue endurance limits that are on the order of six-tenths the static (one cycle) ultimate strength. Hence, over the entire fatigue loading environment and frequency range, the composite can exhibit a six-fold improvement over metals in the $10^6 - 10^8$ cycle range [3]. The larger tensile strength, modulus, and fatigue life of carbon fiber reinforced plastics coupled with the freedom to shape the piece to nearly any complex geometry makes carbon fiber a very desirable frame material.

Table 2. Materials Comparison

MATERIAL	DENSITY (g/cc)	TENSILE STRENGTH (ksi)	SPECIFIC TENSILE STRENGTH	TENSILE MODULUS (Msi)	SPECIFIC MODULUS
Steel	7.8	145	19	29	3.5
Titanium	4.5	134	30	16	3.5
Aluminum	2.8	67	24	10	3.5
Glass Fiber	2.5	246	98	10	4
Carbon Fiber	1.9	228	120	55	29
Aramid Fiber	1.4	385	275	19	14
Boron Fiber	2.6	443	170	23	9
SiC Fiber	3.5	500	143	57	16

Figure 10. Tensile Strength and Modulus Comparison

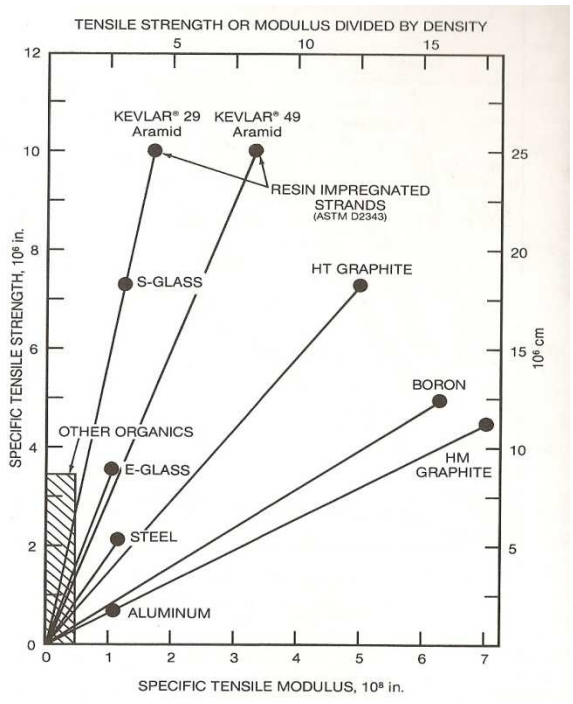

From Figure 10, Aramid fabrics (Kevlar®) display much larger tensile strengths compared to carbon fibers(Graphite). Though the tensile strengths of the Aramid fiber reinforcements are much higher, the specific modulus of this fabric is much lower than that of carbon fabric. The specific modulus is one of our most important parameters, since it will determine the amount of strain that will be experienced per given load. Simply put, the higher specific modulus, the lower the strain for a given load. In order to maximize the riders' input energy translated into forward motion, minimal energy should be lost to component and frame deflection. Therefore, carbon fiber is the optimal candidate for frame material.

Disadvantages of using carbon fiber as our main material were also considered. Carbon fiber is more expensive, more difficult to manufacture, has longer processing times (due to curing of epoxy), requires more planning and preparatory work, and involves more complex analysis in order to achieve the maximum benefits offered by the material. However, these difficulties can be worth the extra considerations for such a substantial increase in performance.

As mentioned previously, the team decided to use existing bicycle components on the market to save time, which was then devoted to the design of the frame and fairing pieces. In order to use standardized components, it was necessary to manufacture inserts that are bonded into the carbon fiber frame. Theses inserts consist of dropouts, head tube cups, and bottom bracket shell. These components were machined from 6061-T6 aluminum. The 6061 alloy is readily available at nearly any local materials supplier, which makes this alloy an exceptional choice for prototyping. Because carbon is electrically conductive, galvanic corrosion occurs with many aluminum and cadmium-plated materials. In our case, the inserts are bonded in place with adhesive, 3M-DP420, which insulates the aluminum from the laminate and makes nickel-plating or painting unnecessary.

In order to obtain the greatest stiffness possible from the frame, the team has chosen to implement the use of a core material. By using a core material, one can significantly increase the stiffness of the laminate without adding significant weight. From Figure 11, the stiffness effects of core material are demonstrated. Core materials can vary widely in acceptable uses, strengths, and weaknesses. Through consultation with experienced individuals from AeroVironment Inc. and extensive research online, a suitable foam material was determined. The core material chosen was Foamular 150, by Owens Corning Sales, LLC. Foamular 150 has the lowest density of foams that were researched at approximately 1.44 lb/ft³. It also has a very small cell structure, for low resin absorption.

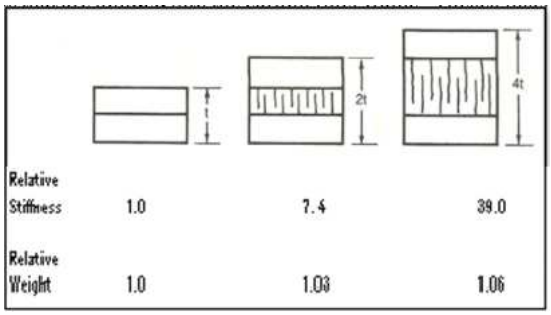

Figure 11. Core Material Effects

Manufacturing Methods: Frame

The foam core of the frame is a fairly complex geometry, and thus presented a manufacturing challenge. Shaping the foam core can be done in a few different ways: by hot-wire cutting and sanding, a CNC foam cutting router, and a CNC five axis machine. Shaping the frame by hot-wire cutter and sanding is the most difficult requires the simplest equipment. CSUN has a CNC foam router, but it can only cut in 2D, thus it would be necessary to cut many separate pieces, and then bond them together. The optimal way to cut the foam is to have the foam cut by a shop with a five axis CNC machine. This alleviates the task of cutting the foam frame that would otherwise require an estimated two weeks to cut by hand. Therefore, the team decided to pay for the foam core to be cut by an experienced foam cutting

machine shop. The foam core was cut in two pieces down the middle from the front to the rear. This allowed the cables to be routed through the frame before bonding the halves together.

Once the foam frame is cut the next step is to hold the frame and the aluminum inserts in place in the exact geometry determined by our solid model. Keeping in mind that future teams might want to adjust the geometry or size of the frame dramatically, the device used to hold all the pieces needed to be adjustable. To hold the frame and all inserts in place, a frame jig was constructed. Unlike jigs for conventional bike frames, this jig holds the frame in such a way that it can be accessed from both sides, allowing plenty of room for a composite layup. Through researching adjustable frame jigs the configuration shown in Figure 12 was discovered. Our jig incorporates the use of t-slot extrusions for quick adjustments as in Figure 8, but uses a different supporting structure. This enables us to wrap the frame from both sides without removal and adjustments between each layer.

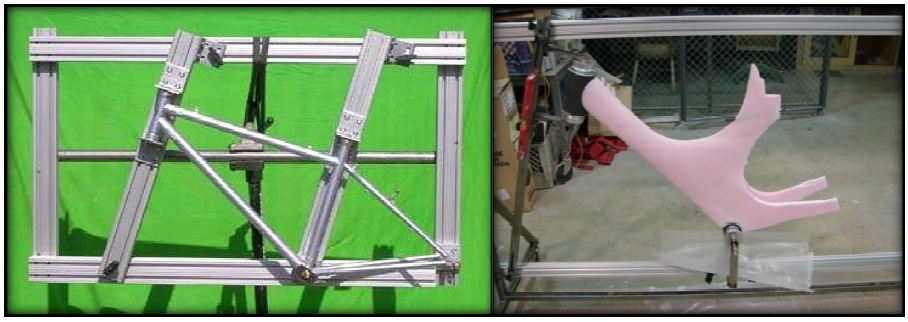

Figure 12. Adjustable Frame Jig

The bottom bracket area was designed as a separate component to be fabricated, inserted into the foam frame and wrapped with the frame as one complete system. The aluminum bottom bracket shell was placed inside a cylindrical container in which the piece was surrounded with epoxy thickened with microspheres and chopped carbon, increasing the toughness of the epoxy, and creating a very rigid structure with a much larger surface area to bond into the foam core. Once the bottom bracket area was fabricated, it was bonded into the foam core in its exact location by the use of the frame jig.

The head tube was constructed by wet-layup without vacuum bagging. An aluminum tube mandrel was cut just under the inner diameter of the designed head tube to allow for the thickness of a wax release layer. The mandrel was then wrapped with the carbon fiber in the desired orientation of [0°, 90°, -45°, +45°]2 one layer at time. After each layer was thoroughly wet out, the layer was compressed using a two inch wide strip of peel ply material wrapped around 1 inch diameter PVC pipe, to aid in applying tension to the wrap. The peel ply was wrapped around the wet out layer spiraling across the mandrel and held tight at the opposite end by duct tape. This process allows for the extra resin to be evacuated from the fabric without the inherent pinching of the fabric on two sides as obtained from vacuum-bagging or molds. The layers were applied in this manner one at a time to decrease the possibility of extra resin being trapped, and to increase uniformity of the dimensions and fiber orientation. Each layer was allowed to cure to about 90% of the suggested cure time at room temperature, at which time the peel ply wrap was removed. A light dry sanding of the layer was then conducted using 400 grit sandpaper, removing any excess peel ply material prior to the next layer. This takes approximately two minutes, since the sanding is only intended to clean the surface, not to change any surface features. Acetone was used to clean the surface after sanding, then the layup of the following layer commenced.

The frame will need to be vacuum bagged since even pressure cannot be achieved around the edges and sides. A quite complicated bag will be trimmed out and placed over and around the fixtures on the frame jig in order to keep the frame mounted in the jig between the start and finish of production so as to keep the desired geometry and alignment fixed. The reinforcement layers of unidirectional carbon will be applied one at a time in the necessary locations of the frame for optimal rigidity in the desired directions. Following the unidirectional fiber application the joints will be wrapped to the desired number of approximately ten or twelve layers to increase the rigidity of the bonding and high stress areas. Subsequently, the two or three cap layers of plain weave carbon fabric will be applied to the entire frame to add strength and smooth the joints and heavily wrapped areas. Once the desired wraps are applied, a single layer of epoxy will be applied to the entire frame surface as a clear coat protecting the fiber reinforcement and improving the aesthetics. This epoxy layer will then be polished to the desired luster before the competition.

Manufacturing Methods: Fairing

Currently, our focus lies on manufacturing the fairing. The fairing will be built using layers of aramid and crows-foot weave carbon fiber. The number of layers is based upon the results of our sample pieces. During the sample process we varied the number of layers, orientation, and weight of fabric used to achieve an optimal weight vs stiffness balance. These results yielded two options: carbon fabric as the outermost layers with a middle layer of Kevlar, or a Kevlar layer as the innermost layer and a carbon outer layer; both would yield a structurally sound outer shell. In the second case, a dye will need to be added to the epoxy to eliminate the need for painting, since Kevlar has poor UV characteristics. Using this

number of layers and not having to wrap fabric into a tubular form allows us to use a mold and the vacuum-bagging method, creating a fast process.

A female mold would have been preferred, as its surface would have been against the mold surface, resulting in an improved surface finish. However, due to the amount of material needed for female molds, time, and facilities, the team was limited to using a male mold for the front and rear fairings. The exposed surface will be left as a peel ply print, and surface treatment will be done afterward. The fairings will mount onto the frame by carbon slip tabs, which will use a rectangular piece bonded to the outside of the frame and a tab bonded to the fairings. This method of attachment will eliminate the need for mechanical joining and expensive titanium or nickel coated hardware. We will be able to use the remnant carbon from the fabrication of the fairing and frame to make all necessary tabs. All composite parts trimming will be done using a reinforced cutoff disc with a Dremel tool due to the complex contours of the edges. The edges will then be protected via plastic tubing halved and adhered to the edges.

The molds were manufactured by using the solid models created in SolidWorks. These files were converted into parasolid files and imported into Esprit, where it was used to create the NC codes. CSUN's three axis CNC foam router used the NC code to cut out sections of the fairing. Due to the travel limitations of the router along its Z-axis, the mold had to be cut in layers, and then stacked and bonded using BJB expanding two part adhesive.

Figure 13. Tail Cone Male Molds

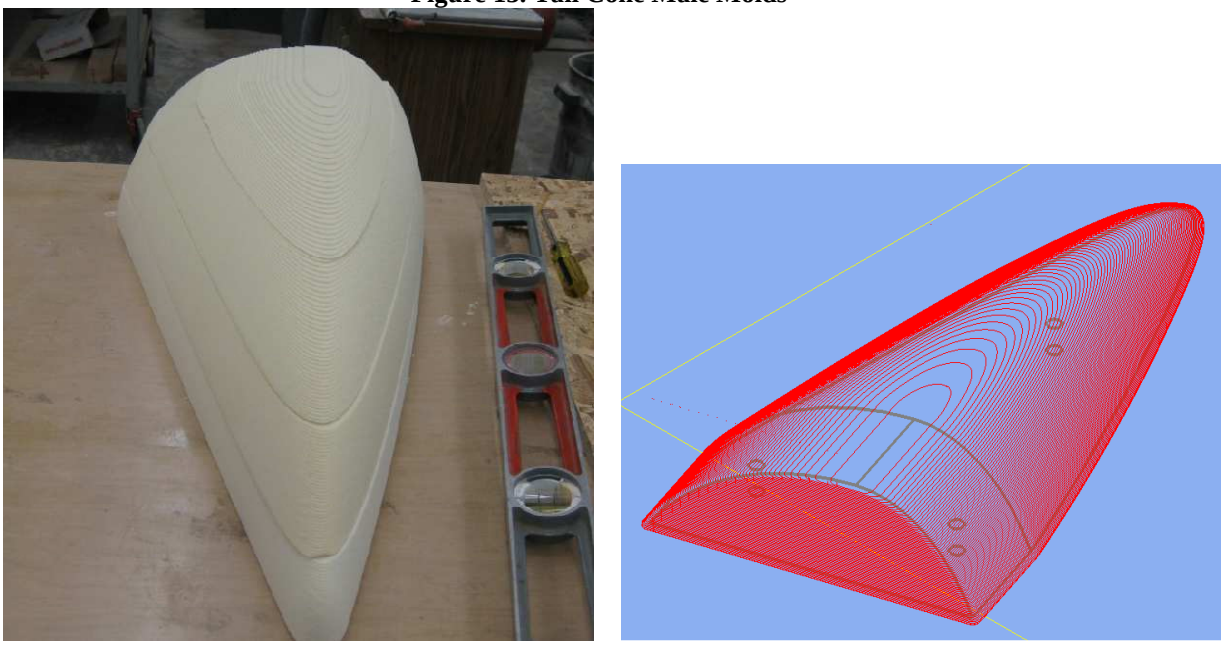

Developmental Testing

In order to properly design and analyze the P.F.C.S.U.2.W.H.P.G.V., the team made it their task to find accurate base line data from standard road bikes. This was accomplished through geometry measurement, accelerometer road testing, power measurement, material testing, body scanning, and motion capture. This data, in conjunction with research, hand calculations, computer based simulations, and additional physical testing, were used to accurately design and analyze a structurally sound, aerodynamic, and ergonomic frame and fairing. The portions of developmental testing not previously discussed are explained below.

Load Distribution

The frame is the largest structural member and single piece of the entire vehicle; all the hardware attaches to it and all loads pass through it. There are also various components that need to be pre-fabricated that get integrated into the frame to make an inseparable assembly. The head tube is the area where the fork passes through a set of bearings and attaches to the handlebars. At the rear of the frame there are aluminum pieces called dropouts that attach the rear wheel to the frame. Lastly, the bottom bracket is the tube area that supports the pedal cranks and associated bearings.

Before a conceptual design could be made, an analysis of the loading conditions needed to be performed on a standard bike. A basic sketch was created based on the fit-bike measurements of all the riders to simulate wheelbase, seat and handlebar distances and height. Using the weight of the heaviest rider, calculations were made of the static reactions on the HPV from the rider and the ground. It was decided to then perform the calculations with the rider in the so-called "aero" position as this provided the most weight transfer over the front tire and would provide for a conservative analysis; this is especially critical because the head tube to frame interface is crucial and a failure at this point would be catastrophic to both the vehicle and rider.

Using a trainer to support the rear wheel, the rider and a standard bicycle were positioned on a scale and used to verify the calculated loads and weight distribution between seat and handlebars. It was found that if the rider's weight is $250lb_f$ then while in the aero position, $160lb_f$ would be concentrated over the handlebars and 90 lb_f would be left acting on the seat. The reactions acting through imaginary vertical lines passing through the front and rear axles and points of contact on the road were found to be approximately $107lb_f$ on the front axle and $143lb_f$ on the rear. With this basic information established, the design team was able to start on a conceptual design while allowing for further, concurrent analyses to take place.

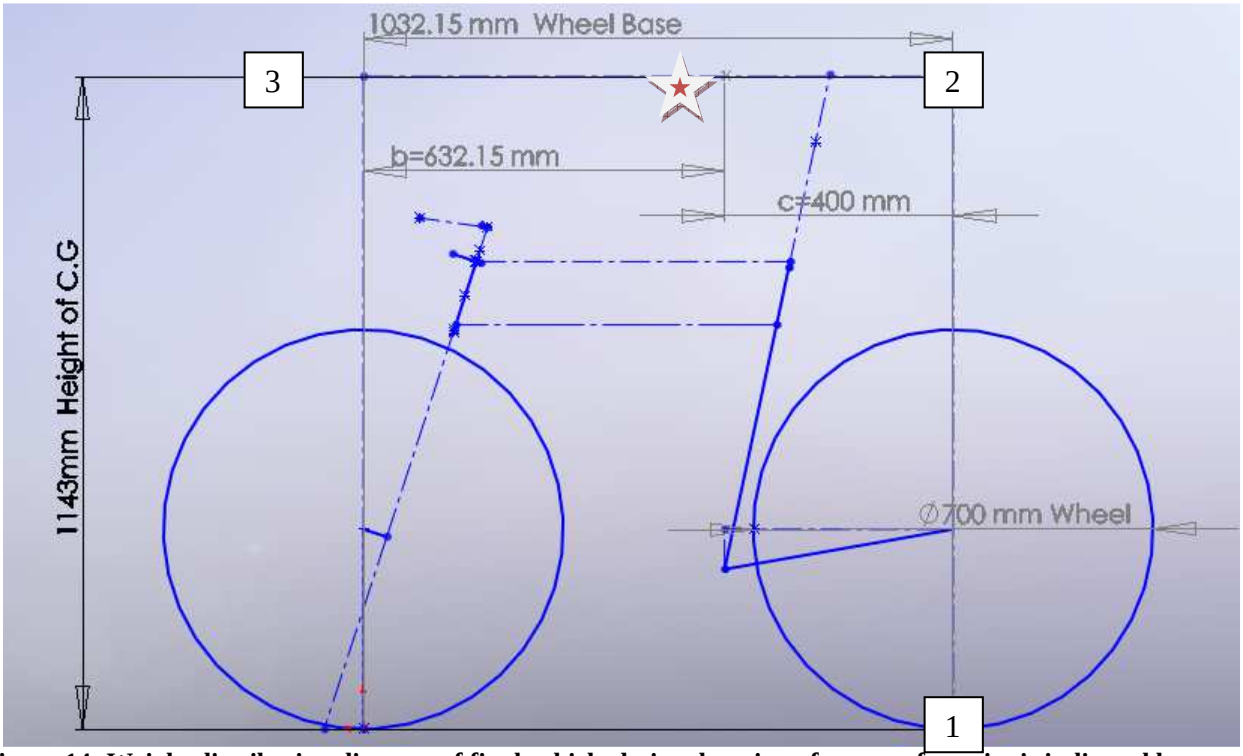

Figure 14: Weight distribution diagram of final vehicle design, location of center of gravity is indicated by a star

Accelerometer G-force Acquisition

As part of the testing program conducted while the design was being formulated, aluminum mounts were fabricated to accept the threaded end of an accelerometer probe, and the other ends made to fit on a standard road bike at the head tube, rear axle and bottom bracket. The accelerometer and mounts were used on several occasions to determine the g's that one encounters during normal riding. After several testing sessions, it was found that during normal riding it was quite common to see readings of around 2 g's and at times readings as high as 5 g's. This information was provided to the design team to aid in the stress analysis of the frame.

Figure 15. Accelerometer Road Test Fixture and Data Acquisition Set Up

Power Test and Race Simulation

To determine the amount of power that our riders could generate under typical riding conditions, a Power Tap® was used to obtain actual data from each of the riders. The Power Tap is a hub which is mounted to a wheel which uses a series of strain gauges to measure torque. The system is equipped with the hub and wheel, a computer receiver, and heart rate monitor (HRM) which send the measured data wirelessly to the receiver. From the Power Tap, the riders' cadence, torque output, power output, distance, and speed can be obtained. This wheel was used in an endurance test and sprint test, where several of the riders were tested and their results analyzed.

The course that was used for this event took place on the Kern River Trail near Bakersfield, California. The event route can be seen on the CSUN HPV website. The total duration of the event was approximately 7 miles with a turn-around halfway. The starting, ending, and turn-around (fork) locations can be noticed in the plot below. The data output from the Power Tap® for one of the riders, during the endurance test, can be seen in Figure 16.

Figure 16. Plot of Power Tap Results for one Rider During the Endurance Test

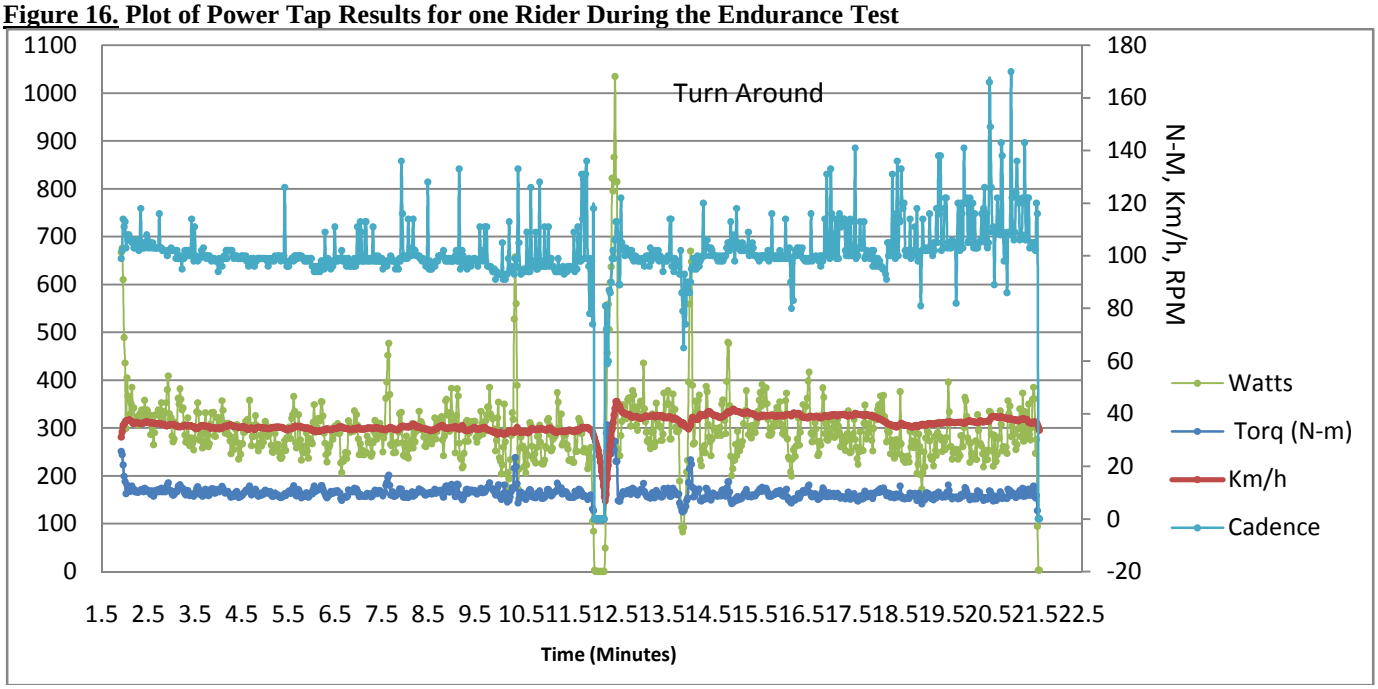

Figure 16 displays the output torque and power and also shows the speed and cadence of the rider. Data was recorded every two seconds. The time at which data is shown corresponds to the start of the course. The data then ends when the riders reach the starting point again. From the plot above, the point where the turnaround occurred is clearly visible, due to the dramatic decrease in speed, cadence, torque, and output power. The peaks indicate the maximum values generated. Immediately after the turn around point, all parameters increase and peak dramatically due to the rider sprinting from almost a complete stop to approach and maintain speeds before the turn around.

The results for all of our riders are summarized in Table 3. The Power Tap had some issues the day of testing which affected the results for one of our riders (Marc) and also the heart rate monitor failed to record and send data. The data was obtained after plotting the Power Tap results and locating the largest peak in each of the parameters.

Table 3. Power Tap Final Results for All Riders For the Endurance Event

Rider	Maximum Power (W)	Average Power (W)	Average Cadence (rpm)	Maximum Speed (km/h)	Average Speed (km/h)	Maximum Torque (N-m)	Average Torque (N-m)	Total Time (min)
Anna	457	193	79	36.752	30.81	19.659	7.44	22.575
Josh	**1345**	270	90	42.107	32.88	**48.809**	**9.84**	20.517
Marc	****	****	****	****	*****	****	****	****
Nick	1035	**273**	**95**	**44.659**	**34.24**	35.816	9.38	**19.677**

The bold values in Table 3 represent the best over-all results from all of the riders. As can be seen, Nick produced the best results in 4 out of the 7 measured outputs which resulted in the shortest time.

A sprint test was also conducted set up similar to the sprinting event in the competition. The course was held on a smooth, straight, level street. The timed portion is approximately 100 meters long, which is preceded by a run-up of approximately 500 meters. Three runs through this sprint test were done by each rider. The Power Tap results of the runs for one of the riders can be seen in Figure 17 The three separate runs are clearly visible by the three power output peaks.

Figure 17. Plot of Power Tap Data for Three Sprint Events of One Rider.

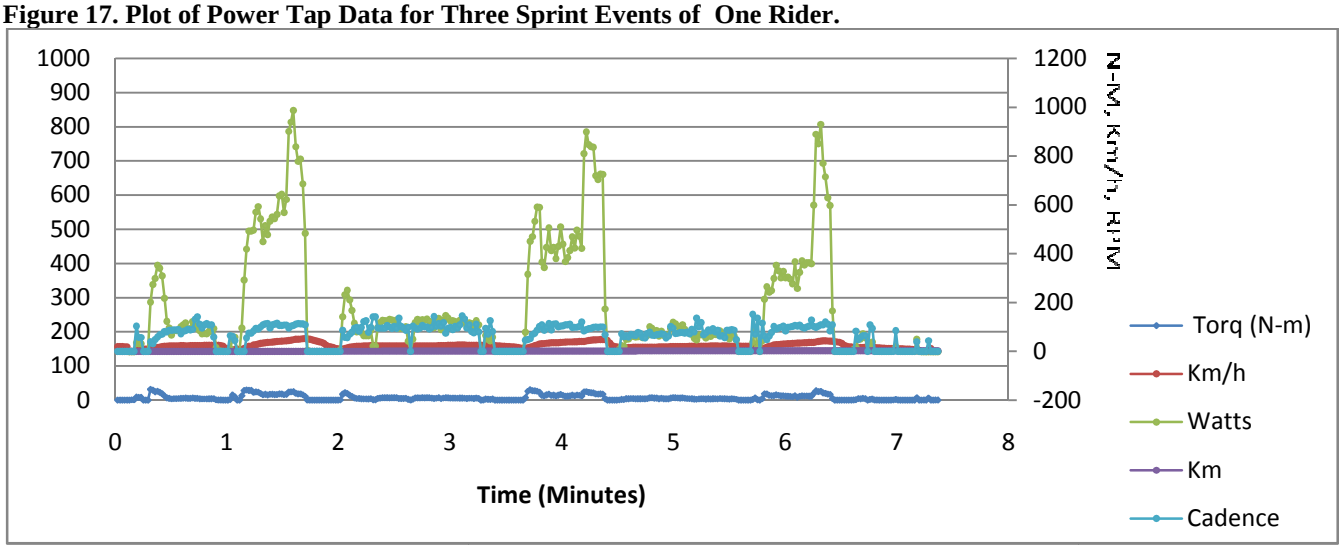

The point where the rider begins sprinting is indicated by a noticeable jump in power output, torque, speed, and cadence. It is interesting to note that the maximum speed and maximum output power do not occur at the same time. The maximum speed is reached several seconds after the maximum power is generated by the rider. This can be seen more clearly in Figure 18.

Figure 18. Power Tap Data for the 100 Meter Sprint Timed Box for One of the Riders.

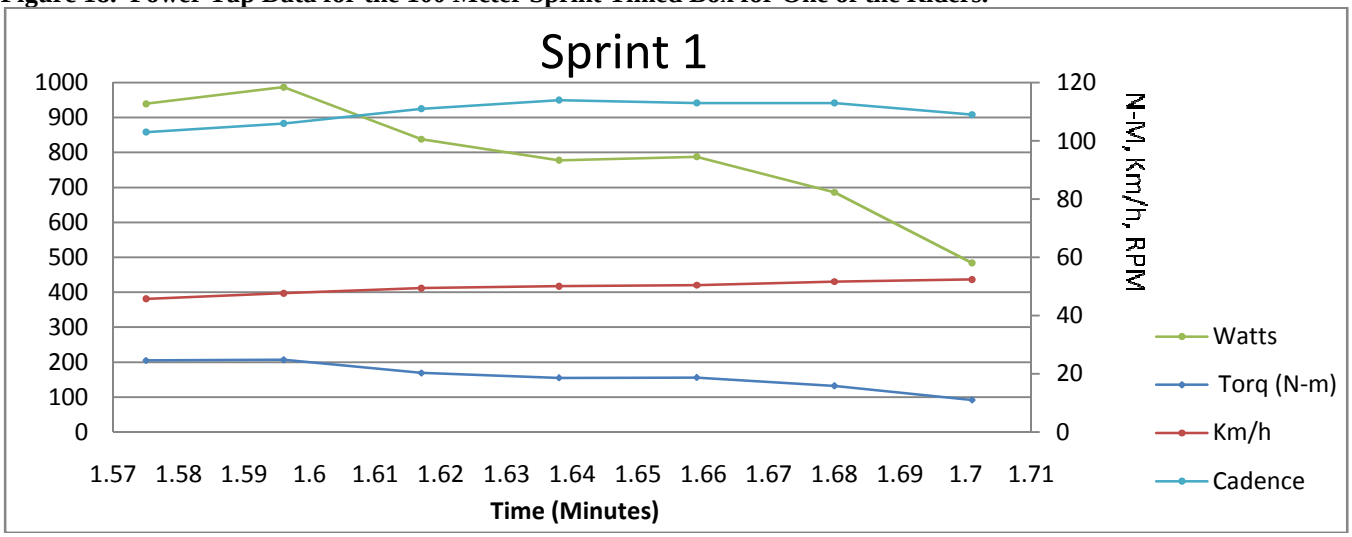

The maximum speed is reached at the end of the 100 meter timed box. The total time duration to pass through the timed box and the maximum speed can be seen in Table 4 for one of the riders. The bold value represents the fastest speed.

Table 4 Sprint Results for One Rider for Three Sprinting Events, No Fairing.

	Total time (sec)	End speed (km/h)
Sprint 1	7.56	**52.447**
Sprint 2	7.56	48.639
Sprint 3	10.08	43.092

As mentioned, the testing discussed thus far was conducted on an upright bicycle. The sprint test was then performed on a recumbent bicycle on the same course for comparative purposes. In Figure 19 the results of the test for the recumbent can be seen, for the same rider used in Figure13.

Figure 19. Recumbent Sprint Test of One of the Riders

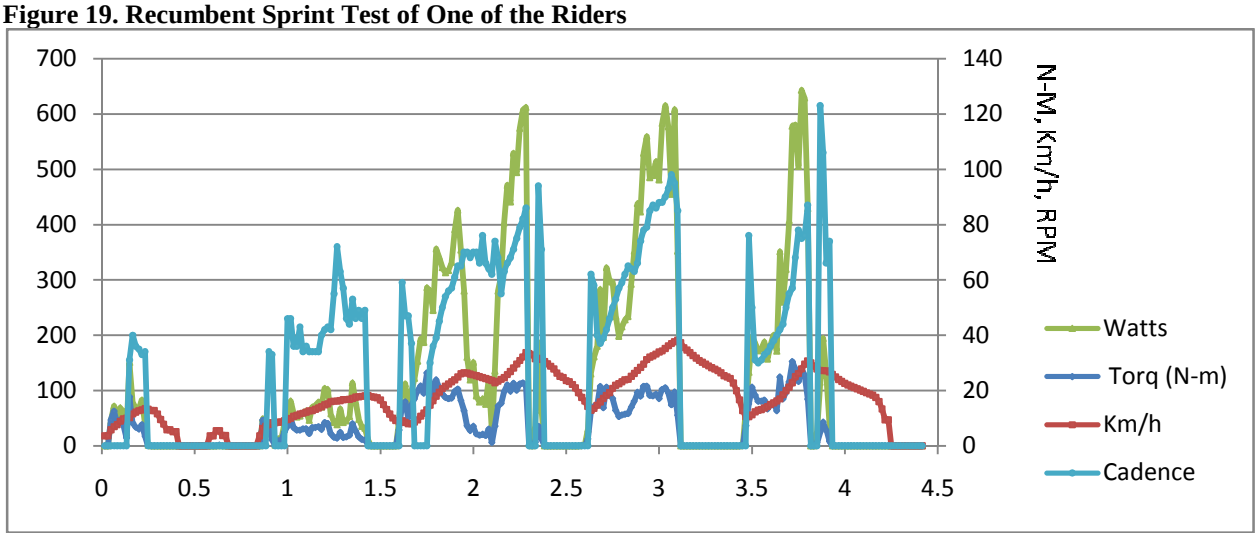

Comparing the results shown in Figure 19 with those of the upright sprint shown in Figure 17, a dramatic difference can be seen. The maximum power generated on a recumbent is much less than the power that can be produced while on an upright bicycle. Table 5 shows the results of both tests.

Table 5 Maximum Speed and Power Output for Upright and Recumbent Vehicle in Sprint Event.

	End Speed (km/hr)	Max Power (W)
Upright	52.47	987
Recumbent	38.18	643

The testing using the Power Tap described above was also performed by an average non-cyclist female college student. The endurance course was exactly the same as that used for the other riders; however it was approximately half the distance. The resulting plot of data obtained from the Power Tap® is shown in Figure 20

Figure 20. Plot of Power Tap Results for Average Female Rider During Endurance Test

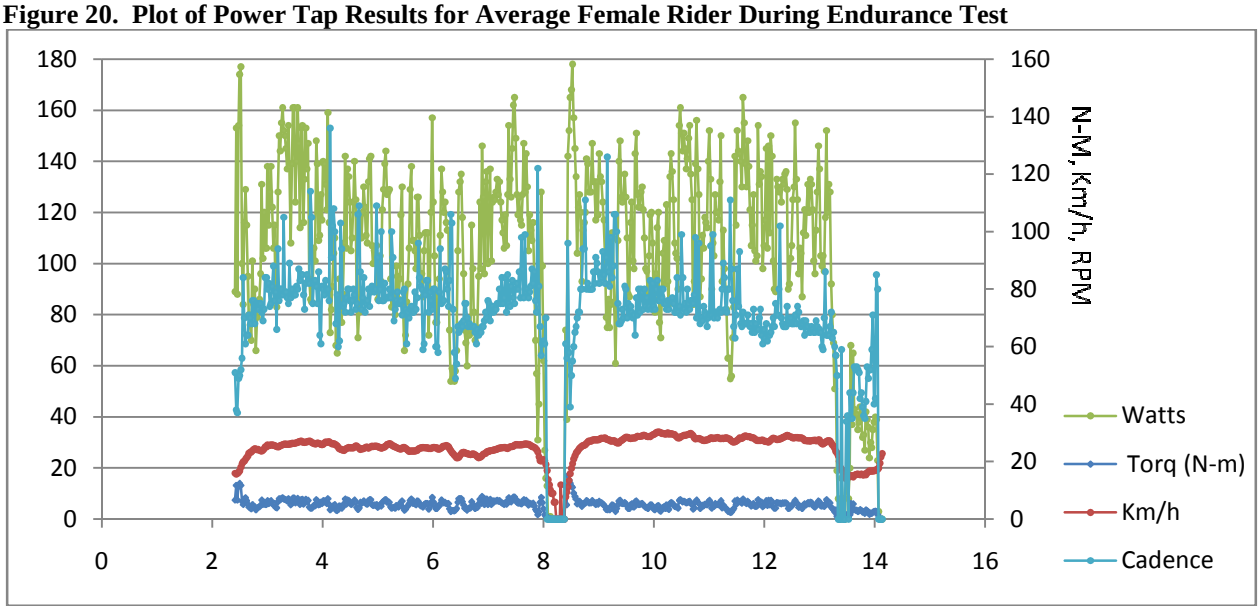

As can be seen in Figure 20, the variations in output are much more dramatic and uncontrolled compared to that obtained from the rider shown in Figure 16. The average values are also much lower, with the maximum output power not much more than the average power. This rider also completed three sprint events. The plot of this data is shown in Figure 21 below. Similar results were obtained in this event. The final top speed and maximum power were significantly less than those produced from the other riders. These results are expected since this rider has had no prior training and exhibits average bicycle handling and pedaling skills.

Figure 21. Power Tap Results for Average Female Bicycle User in Three Sprint Events.

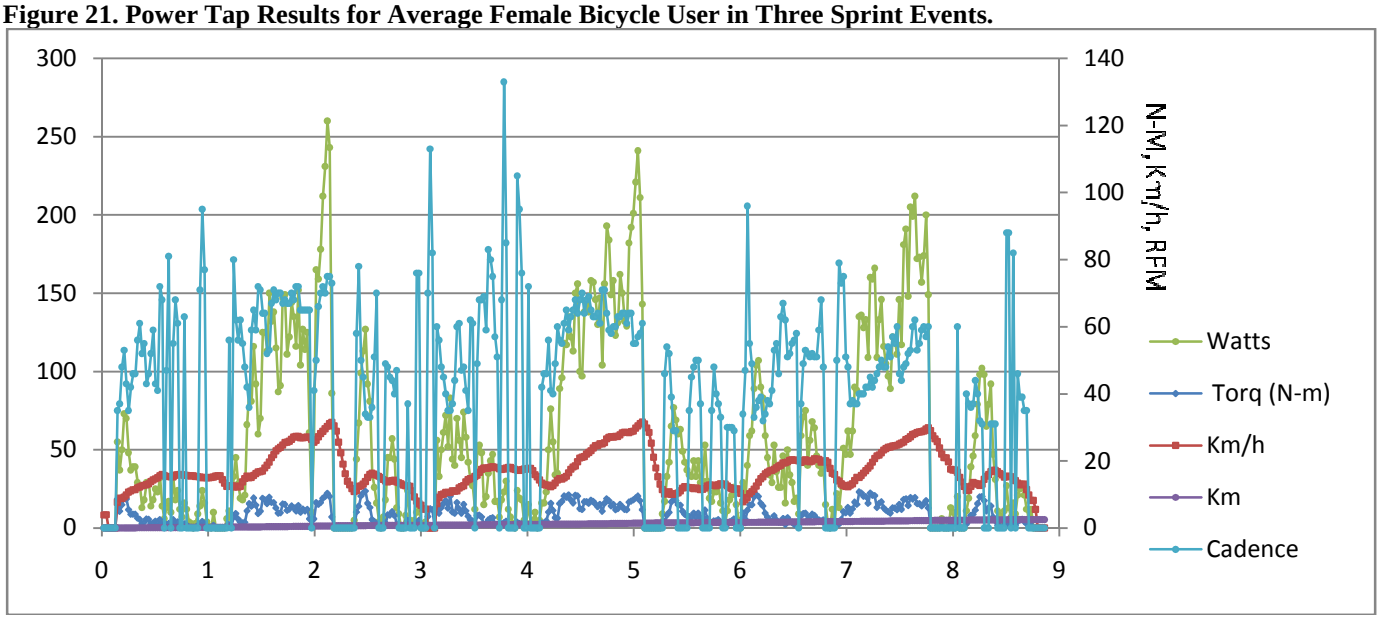

Composite Testing

As with the aluminum parts, in order to perform an accurate analysis it was necessary to know the material and subsequent material properties. Due to the nature of carbon composite and the endless possibilities for weave/resin combination, it was first necessary to define the specific material properties of the carbon and resin combination used. To do this, three batches of twenty total sample pieces were constructed and a tested to failure in a tensile test machine. The data was collected in a spread sheet and all the critical parameters calculated. Averages were calculated for the shear stress, strain, and Young's modulus; Poisson's ratio was assumed to be 0.4 and stress v. strain graphs was created. Seen in the figure 22 is a typical stress v. strain curve from the tensile test data, and below it is the tabulated average material properties calculated from the test specimens.'

Figure 22: Typical stress v. strain plot of test specimens Values Note: The small irregularity in the curve indicates failure of a single fiber

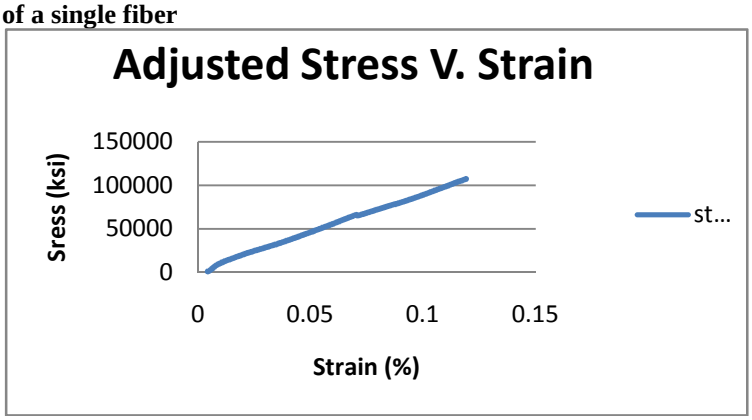

Table 6. Mean Material Property

AVG	Carbon Test Strands
Stress	109.32 KSI
Strain	0.1428
Young's Modulus	776.627 KSI
Shear Modulus	206.035 KSI

Analysis

Aluminum

Once the conceptual design was complete an analysis was done to optimize the pieces for strength and weight. Starting with the aluminum pieces to be manufactured, the dropouts were analyzed. The specific alloy chosen for these pieces was AL ALY 6061-T6. With a requirement of a safety factor of at least 2.5 at yield, the solid models were meshed, constrained and loaded in COSMOSWorks and then analyzed. For the loading conditions, the static reaction at the rear wheel of 143lbf was used, or 71.5lbf bearing load where each dropout meets the axle. This process was repeated several times until the requirements were met by "tweaking" the model after each analysis. Figure 23 shows the final results of the dropout design.

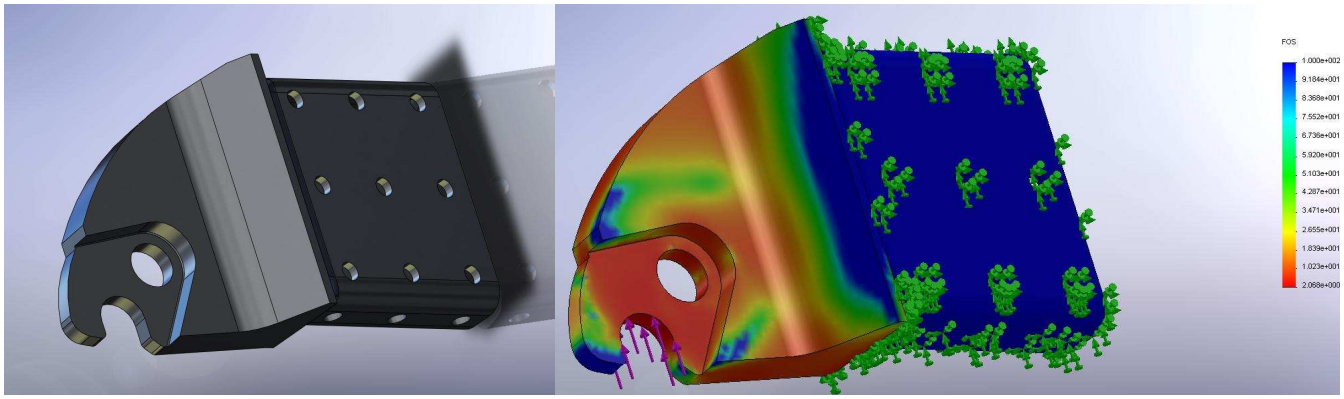

Figure 23: Right Rear Drop Out

The head tube assembly was designed as a pre-manufactured sub-component to be integrated into the frame. It was designed as a carbon tube with bonded upper and lower bearing cups. These cups will also be machined from AL ALY 6061-

T6 and will be lightly bonded in to maintain alignment only. The preload on the headset bearings will be sufficient to keep them in place. Additionally, there are two aluminum eccentrics that allow for an adjustable head tube angle without binding through the full range of turning, and they are compatible with commercially available forks.

The set of four aluminum head tube pieces were also analyzed in the same manner as the dropouts, using the same requirements. The load set was created by resolving the handlebar load and reaction at the front wheel into normal components in relation to the head tube center axis. At the top a load of -159lbf along the axis with a bearing load of 13.9lbf was applied, and at the bottom, a load of +100.5lbf and bearing load of 36.6lbf was applied. Due to design restrictions there was little room to optimize the size and weight of these pieces, however, they were held to at least a 2.5 safety factor.

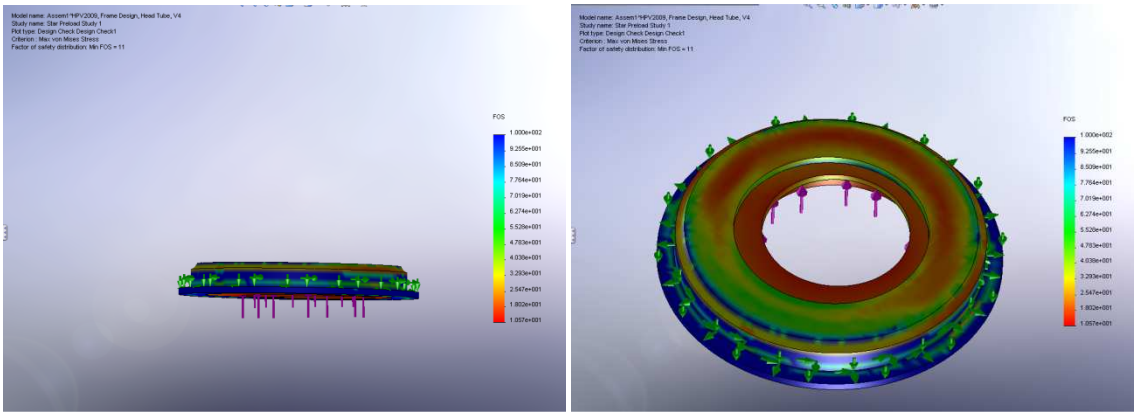

Figure 24. Solidworks Cosmos (Head Tube Pics)

Carbon Frame

The next step was building an analysis model in Femap from the solid model designed in SolidWorks. A parasolid file was made of the foam frame with the aluminum dropouts and the carbon portion of the headtube assembly. With the geometry imported into Femap via parasolid and the material created, the meticulous task of meshing the entire surface area where the carbon was to be wrapped was done. Due to the complexity of the design, professional guidance was sought to ensure the analysis was done properly.

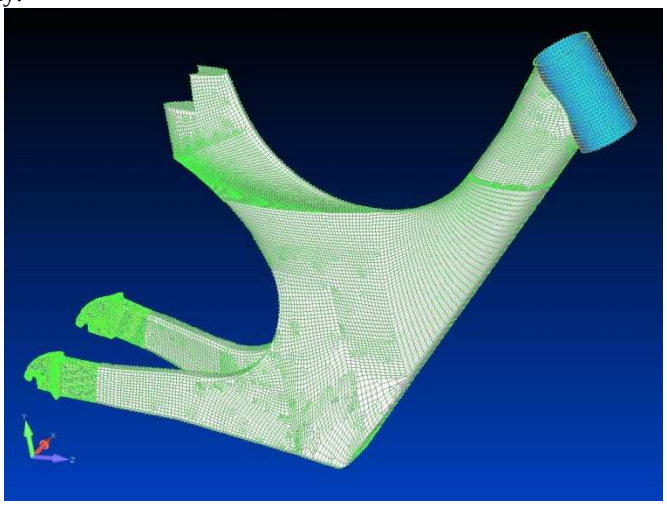

Figure 25: Completed mesh of frame assembly

Next the load cases were modeled. In order to accurately model the concentrated load from the handlebars, a point was created where the stem clamps the bars and a rigid element attached between the point and the head tube. The point load of 160lbf was then applied to the point and rigid body, and 90lbf was distributed about the seat. With the load case for the "aero" position set, the boundary conditions were modeled. Since the analysis is for the static loading condition, the rear was pinned and the front is left as a roller, or wheel. This means that the rear dropouts were literally pinned about the axis of the axle. The fork was modeled as a straight, rigid element attached to the bottom of the head tube following its axis with a spring connecting the end to a node representing the front axle.

Before exporting a data set to be solved in MSC NASTRAN, a geometry check was done. The net effect of this process was twofold: first it provided a check to make sure all the components of the assembly were modeled correctly in Femap and reflected the design intent, and second it acted as a modal analysis. The results yielded ten modes with a range of 14.7-344 Hz and corresponding strain energy plots. The first mode, at approximately 14.7 Hz, is shown in Figure 26; the deformation is exaggerated to provide a better visual reference. The green areas show the higher strain energy concentrations and the pink areas represent lower strain energy.

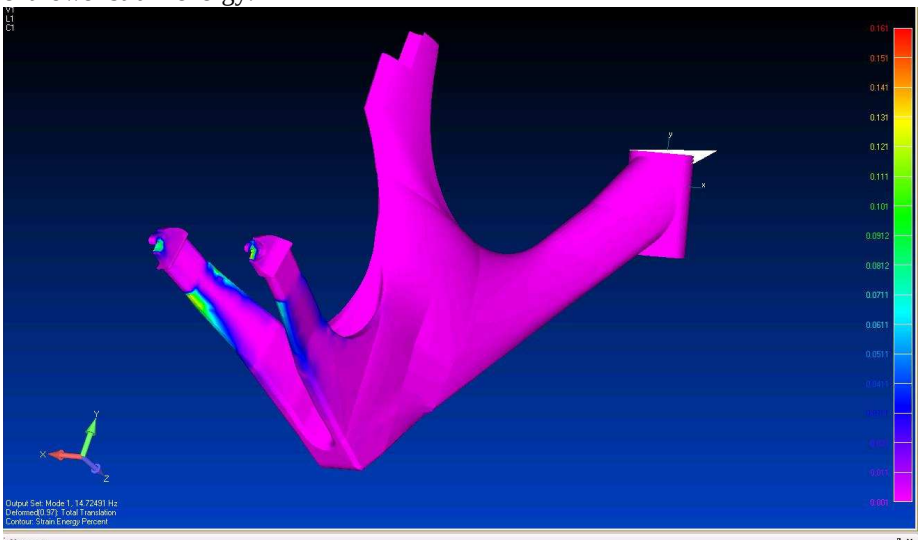

Figure 26: Strain energy plot of first mode, or natural frequency

With the satisfactory results of the geometry check, it was possible to move on to a stress analysis. The same program, MSC Nastran, was used to solve the data set. As stated before, the rear was constrained by pinning the rear axle and the front via a rigid body and spring attached to the head tube and front axle, respectively. The loading case was the aforementioned "aero" case with 90lbf distributed about the seat and 160lbf on the handlebars represented by a point and rigid body. After running the analysis several times and "tweaking" the number of layers, it was determined that at least 15 layers of carbon was needed to achieve a safety factor of at least 1.57. Further analysis is being done to determine the number of layers necessary to raise the factor of safety to around 2.5 respectively.

The second load case to study was the static loading with the 2-5g's measured through the accelerometer testing. These accelerations were caused by imperfections in the road, small cracks, speed bumps, dips, and potholes; in other words, they were measured shock loads. The nature of shock loading is very complex and hard to account for accurately without extensive testing and complex analyses. Instead of directly analyzing the shock load scenario, the team looked for a way to qualify the design for impacts at up to 5g's. This was done by modifying the static aero position load case to be a constant load multiplied by 5g's. The goal being that if the analysis shows a factor of safety of at least 1 at a constant 5g's of the load, then the vehicle will be able to sustain a shock of up to 5g's without any difficulty.

Braking Analysis

In order to account for as many loading conditions as possible, a braking analysis was also conducted. This analysis was purely theoretical and therefore, certain assumptions were made to simplify the process. The assumptions were as follows:

- The total weight of the vehicle and heaviest rider is 250 pounds
- A 40/60 weight distribution for the vehicle in a static state. Center of gravity is placed directly in line with the bottom bracket of the crank set.
- The height of the center of gravity is 45 inches (1143 millimeters) from the ground
- The wheel base length is 39.89 inches (1013.22 millimeters)
- The brakes will apply a constant braking force.
- The minimum braking requirement of stopping within a distance of 20 feet, traveling at a velocity of approximately 15 mph will occur on a flat surface.

To calculate the minimum braking force required to stop the vehicle within the ASME regulations, the following equation was used:

$$F_{B,Min} = \frac{1}{2} * Vehicle\ mass * \frac{(Vehicle\ Velocity)^2}{stopping\ distance} = 93.94\ lb_f$$

This $F_{B,Min}$, minimum braking force, was then computed into a deceleration rate D_X:

$$D_X = \frac{F_{B,Min}}{Vehicle\ Mass} = 12.1\ ft/s^2$$

$$G's: \frac{F_{B,Min}}{Vehicle\ Weight} = 0.376\ g's$$

In order to understand the distribution of the braking forces applied to each wheel of the vehicle, the assumptions about the weight distribution and center of gravity height were made. These assumptions were referenced from the book *Bicycle Science*, written by David Gordon Wilson, and shown in Figure 14. Typically, the weight distribution on an upright bicycle is split at the vertical centerline that the bottom bracket creates on the frame. For the base frame design, the location of the bottom bracket, chainstay or swing arm length, and wheel base were designed for the current riders. The static weight of the front and rear wheel were calculated as follows:

$$W_F\ (STATIC) = 98.70\ lb_f \quad W_R\ (STATIC) = 151.30\ lb_f$$

When the vehicle undergoes $F_{B,Min}$, the weight will transfer from the back of the vehicle to the front. This weight transfer effect for the front wheel was calculated by summing the moment forces of the rider and vehicle weight, the braking force, and the weight of the front wheel in the dynamic braking state, about point 2 in Figure 14. This calculation is shown below:

$$W_{R,D} = 250\ lb_f - 204.69\ lb_f = 45.35\ lb_f$$

The results shown above provide a very important detail; under minimum braking requirements, 82% of the weight is shifted to the front wheels, leaving only 18% on the rear. The thought of running a single rear brake to reduce any weight or aerodynamic drag force would render the vehicle unable to stop in compliance the competition requirement.

The maximum amount of deceleration that the vehicle and rider can withstand without tipping forward was computed by setting the weight reaction on the rear wheel to 0 lb_f and computing the summation of forces about point 3 in Figure 14.

$$D_{X,Max} = 17.28 \frac{ft}{s^2}\ or\ 0.536\ g's$$

$$F_{B,Max} = 134.11\ lb_f$$

The braking torque is related to the braking force through the radius of the wheel. The wheel to be used is 700mm in diameter resulting in a minimum braking torque of 88.32 ft-lb_f for the front wheel and 19.55 ft-lb_f for the rear. The caliper brake system that is common on most bicycles will be incorporated into the vehicle design. This design can be modeled as a disc brake system as shown in Figure 28. The braking disc is the vehicles rim, and the cantilever brake pad is the disc brake pad that is providing the normal force on the rim. The coefficient of friction between the vehicles rim and the SRAM red brake pads was assumed to be 0.5. The radius of the disk where the brake pads will be applied was placed 0.25 inches below the top of the rim, resulting in R_D =17.47 inches (1.46 ft), with a pad surface area of 0.75 in^2.

The minimum brake pressure for the front wheel was computed with the following formula:

$$T_{B,F} = 88.32\ ft - lb_f = 2 * 05 * 1.46 ft * 0.0052\ ft^2 * P_B$$

$$P_{B,F} = 80.91\ psi$$

Similarly the rear wheel brake pressure under minimum braking force and torque was computed to be 17.91 psi. Figures 29 and 30 graphically depict the braking pressure needed, for the front and rear wheel under different decelerations and combine vehicle and rider weights, to stop.

Figure 28: Free Body Diagram for the Braking System.

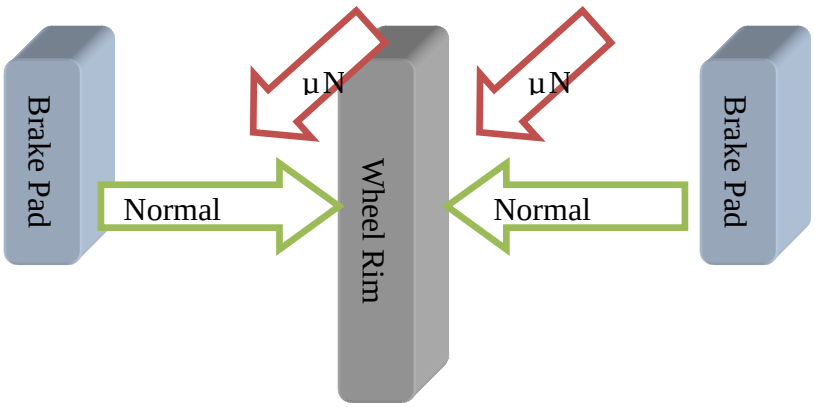

Figure 29: Minimum To Maximum Values of Deceleration Versus Required Brake Pressure for the Front Wheel.

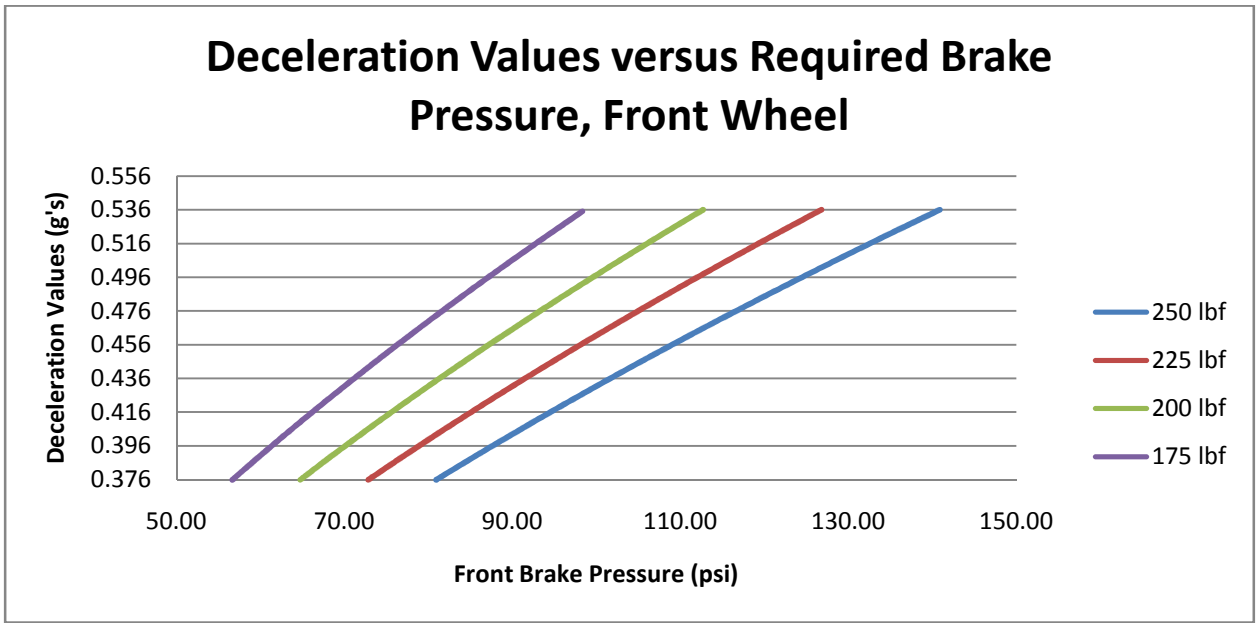

Figure 30: Minimum to Maximum Values of Deceleration Versus Required Brake Pressure for the Rear Wheel.

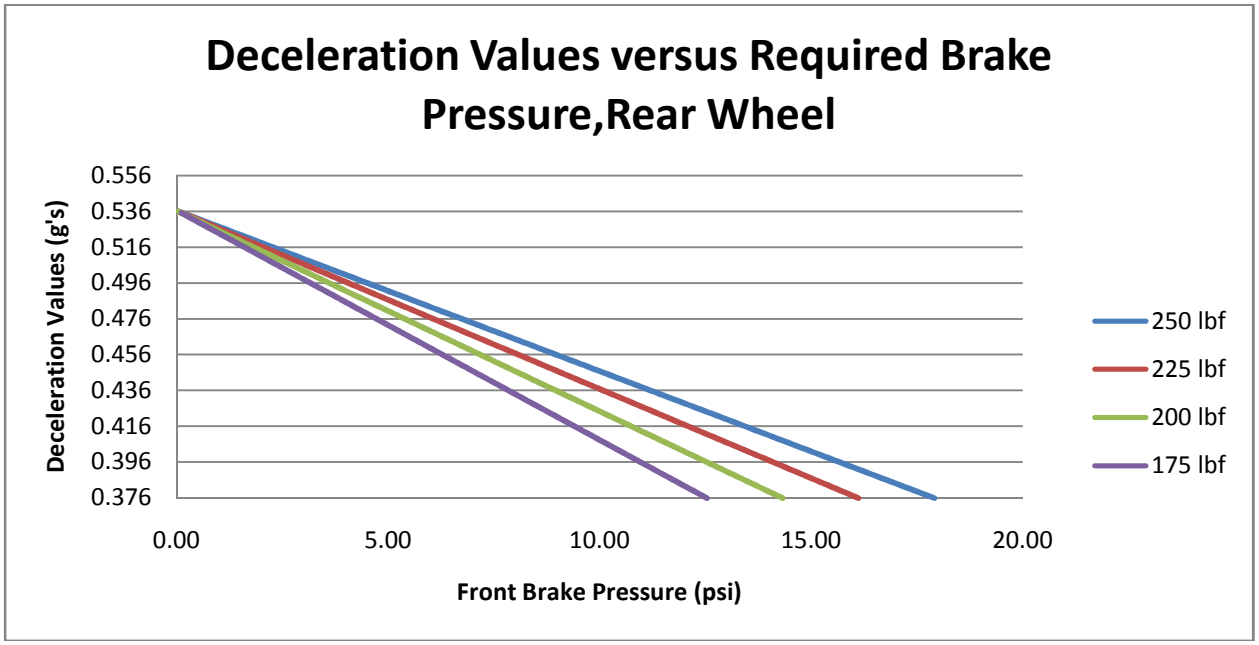

After careful consideration of the results of the braking analysis and the information that it provided, it was decided not to use the brake loading as a separate load case for the finite element analysis. The team felt that the load cases that were run would exceed the loads encountered during braking and would therefore be accounted.

Aerodynamics

In an attempt to predict the performance of our vehicle, an aerodynamic analysis was completed. The analysis uses the simple drag equation to model the total aerodynamic drag on the vehicle. Reynolds numbers were calculated based on a buff body with the characteristic length being the length from the bottom bracket to the top of the riders head and for a streamlined body with the characteristic length being equal the length of the bike from nose to tail. The Reynolds numbers in

each case were found to be 297,000 and 455,000, respectively. Therefore, the majority of the flow is assumed to be turbulent and the simple drag equation applies. Based on the simple drag equation, the frontal area and drag coefficient are key parameters in the total amount of aerodynamic drag. For this reason it was extremely important to attempt to minimize both parameters.

Figure 31 displays the how the total aerodynamic drag changes with frontal area. It is apparent that the drag increases linearly with increasing frontal area. Perhaps a more important observation is that the drag coefficient has a drastic effect on the total drag, for any value of frontal area.

Figure 31. Drag vs. Projected Frontal Area

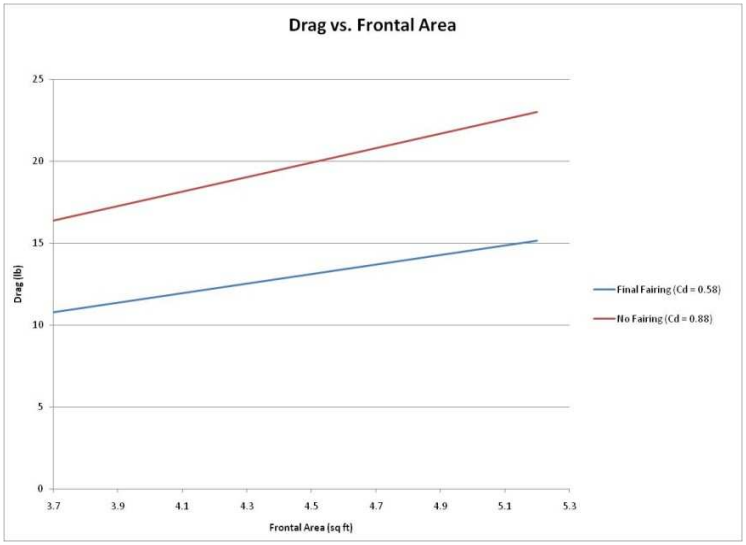

Figure 32. Drag vs. Velocity

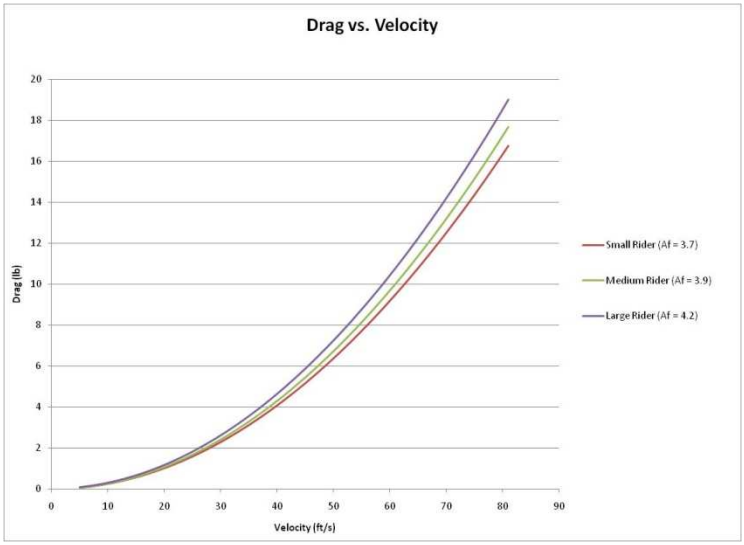

Figure 32, displays how the total aerodynamic drag changes with velocity. It is apparent that the aerodynamic drag increases exponentially with increasing velocity. Similar arguments regarding the importance of the drag coefficient from Figure 32 can also be applied here. Due to the quadratic relationship between drag and velocity, there exists a velocity such that the drag is increasing so rapidly that an effective limit on vehicle speed is introduced.

Initial Predictions where made using the US standard atmospheric model with an elevation of sea level, a frontal area of 4.098 square feet, and an assumed drag coefficient of 0.65 the total aerodynamic drag force at the target sprint speed of 65 ft/s (44.3 mph) was calculated to be 13.39 lbs. Taking into account rolling resistance from the simple rolling resistance model, the total drag force increases to 14.14 pounds. Given this total drag force, a power required to reach the aforementioned speed can be calculated. At the target sprint speed of 65 ft/s 1245 watts would be required disregarding drive train efficiency and 1268 watts accounting for a drive train loss of 2%.

Figure 33, displays how the power required changes with the calculated frontal area. It is apparent the horsepower required increases linearly with increasing front area.

Figure 33. Power Required vs. Frontal Area

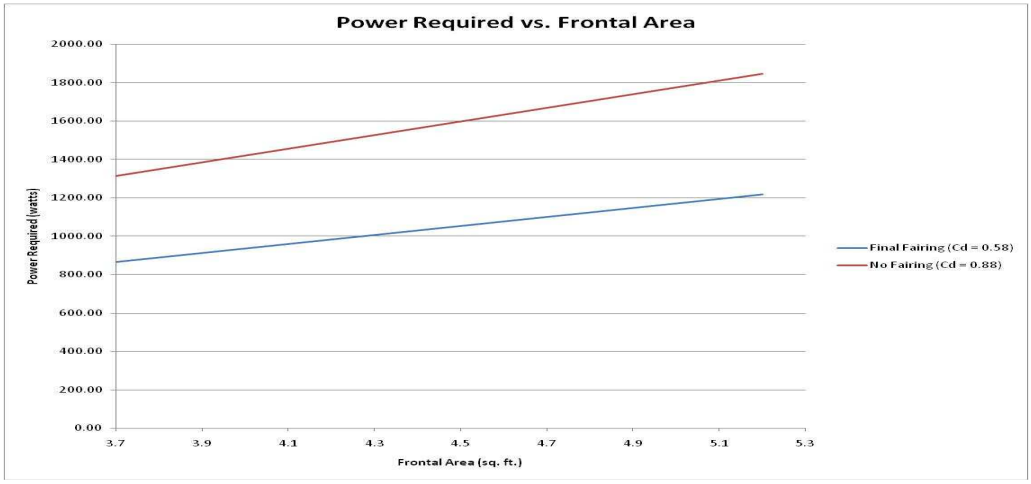

CFD analysis was done using the body scans of three of the riders. These riders were indicative of the "small" "medium" and "large" size riders that would be competing in the HPV Challenge. Using FloWorks, the final fairing choices were analyzed. The leading design was selected based on its FloWorks drag forces at multiple input wind velocities. Figure 34 displays the first of two fairing choices, and its

Figure 34. First Fairing Design

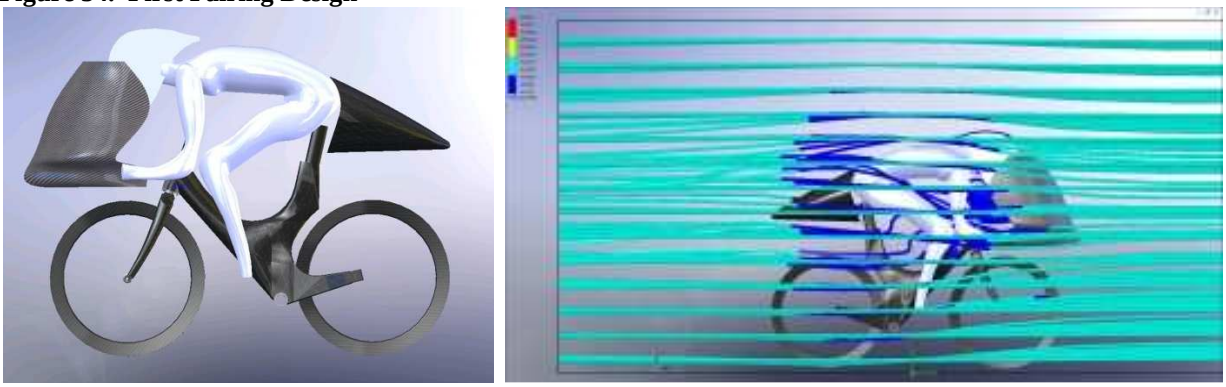

FloWorks simulation. The first fairing was designed to divert the flow up and over the riders head in the vertical direction and around the rider's hands in the horizontal direction, thus completely cover the rider. However, due to geometric constraints the fairing was fairly blunt. Figure 35 displays the second of two fairing choices.

Figure 35. Second Fairing Design

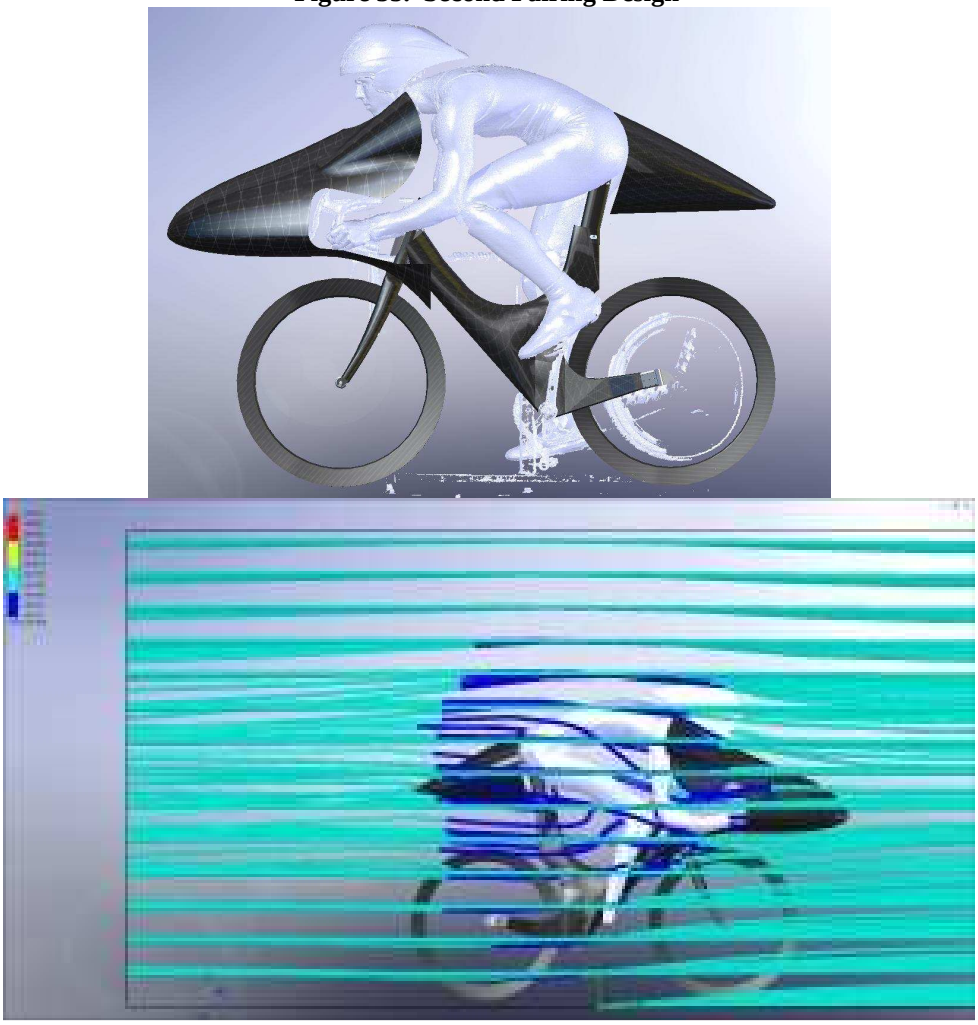

The second fairing was designed to minimize frontal and wetted areas while maintaining safety and practicality. Due to the limited frontal area of the head and the use of aero-helmets, the rider's head was not faired. Instead, the front fairing was designed such that the air flows smoothly up and over the shoulders and torso while the head stays exposed to the free stream. Thus, the frontal and wetted areas, as well as the structural, weight are kept to a minimum. Similarly, instead of increasing the width of the fairing to cover the rider completely, bodily protrusions such as the shoulders are covered through the use of blisters in order to minimize the frontal and wetted areas. The final geometry of the various cut outs may differ from Figure 35 depending on rider-fairing interference. Table 7 displays the aerodynamic drag force of the two fairing designs.

Table 7 – Aerodynamic Drag Force

Design	Velocity (mph)	Aerodynamic Drag Force (lbs)
1	33	6.26
	40	8.43
	45	10.84
2	33	5.68
	40	8.07
	45	10.21

From Table 7 it can be shown that design two has the leading aerodynamic characteristics, and was consequently chosen as the final fairing. For the final fairing, further analysis was done. The frontal area determined via SolidWorks, and the drag force at multiple velocities, shown in Table 7, were used to calculate the vehicle and rider's drag coefficient, and the subsequent power required to attain target speeds. With these new drag forces from Floworks, an updated drag coefficient was calculated and a new top speed predicted. From our most current analysis it is estimated that the drag coefficient of our vehicle is **.58** and our top speed will be **60.5 ft/sec or 41.2 mph** with **900** watts input power. Figure 36 compares the power required for each rider to achieve specific velocities, with the final fairing and with no fairing.

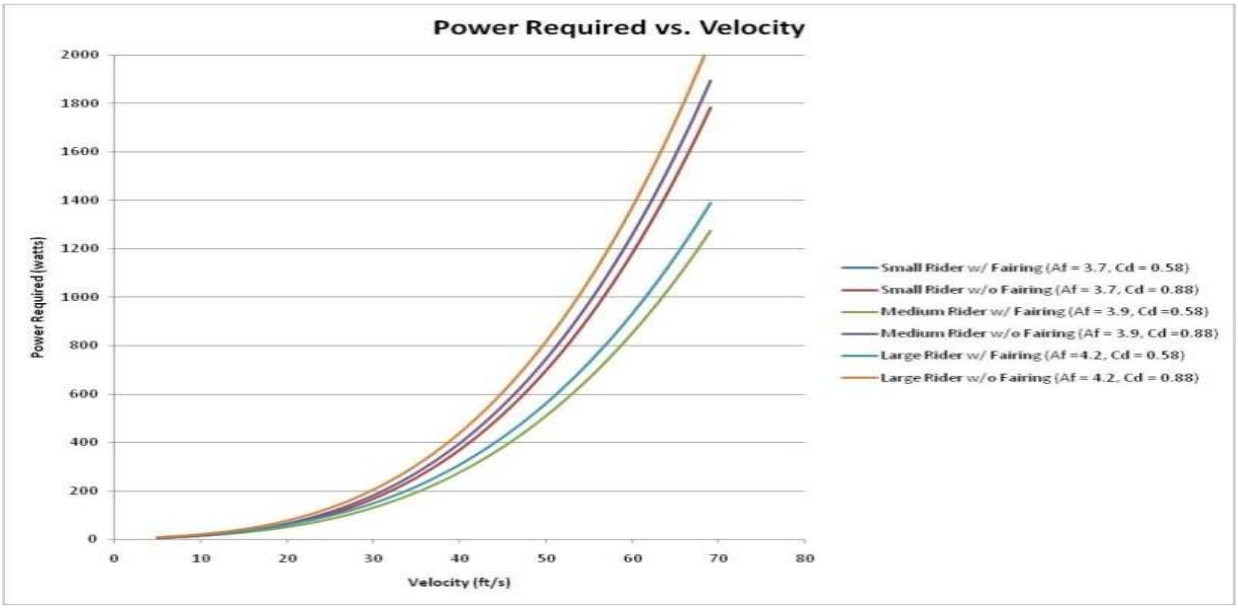

Figure 32. – Sm, Med, Lg Power Required vs. Velocity With and Without Faring

From Figure 36 it is apparent that the power required increases exponentially with increasing velocity for all riders and configurations. In fact a cubic relationship exists, where incremental increases in velocity result in a threefold increase in the power required to achieve the increased velocity. At high speeds the drag coefficient becomes increasingly important as aerodynamic drag quickly becomes the largest resistive force.

Figures 37 through 39 demonstrate power required vs. velocity for the small, medium and large riders as well as each rider's output power at various states of exertion. The intersections of the horizontal lines and cubic curves correspond to each rider's calculated maximum, 5 second sustainable, 30 second sustainable, and infinitely sustainable speeds. Power outputs used in the figures below were determined from the power analysis discussed previously. The drag coefficient of 0.58

represents the calculated drag coefficient for the small and medium rider on the final vehicle design. These drag coefficients were calculated based on total drag forces obtained from the Flo Works analysis, as discussed above. The drag coefficient for the unfaired bike and rider was estimated to be 0.88 [4], obtained from Bicycling Science and represents the drag coefficient for an "average" sized rider in a crouched racing position on a "standard" upright race bike.

Figure 37. Small Female Rider's Expected Speed Range

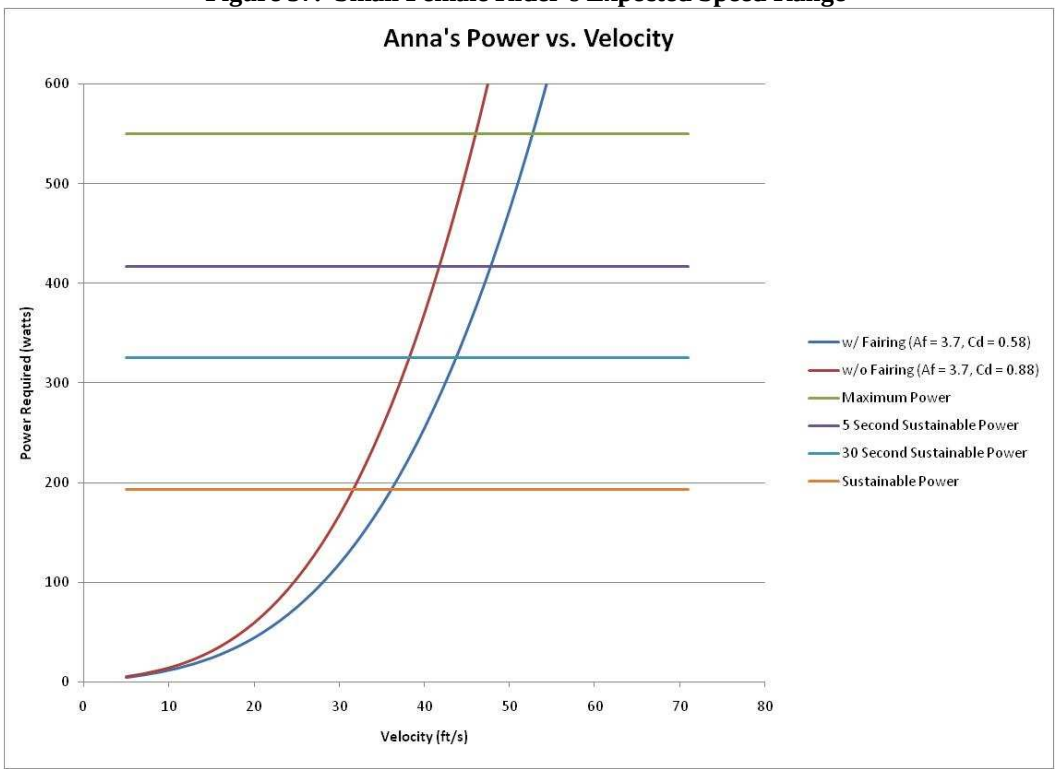

Figure 38. Medium Male Rider's Expected Speed Range

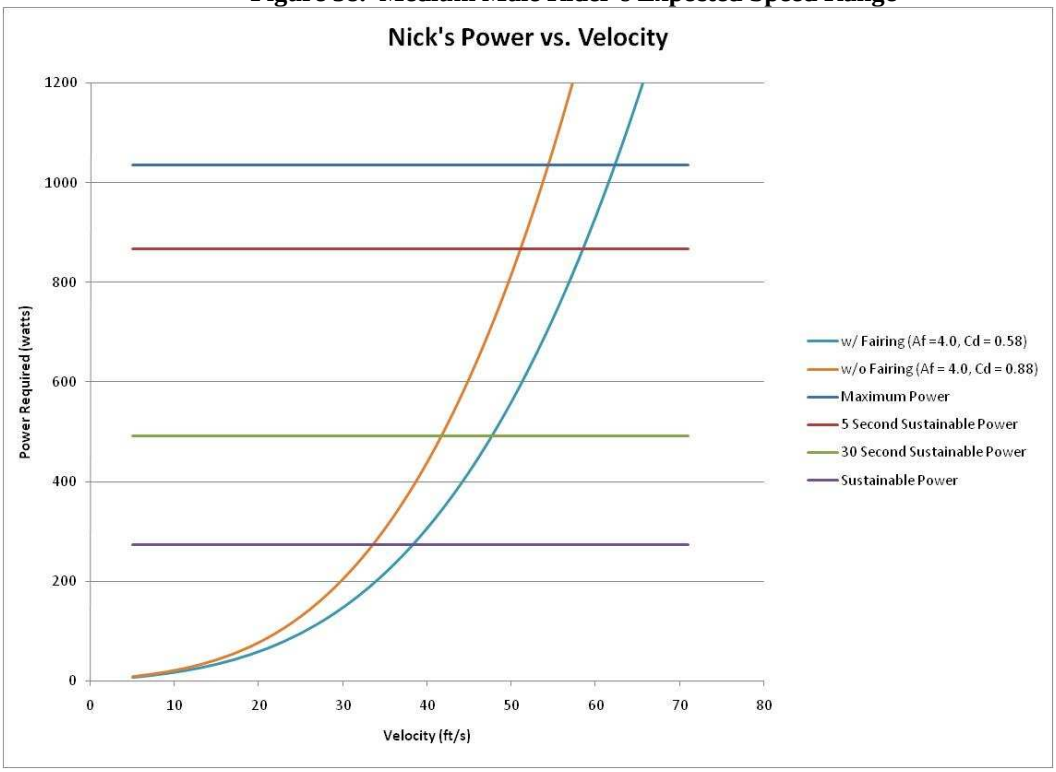

Figure 39. Large Male Rider's Expected Speed Range

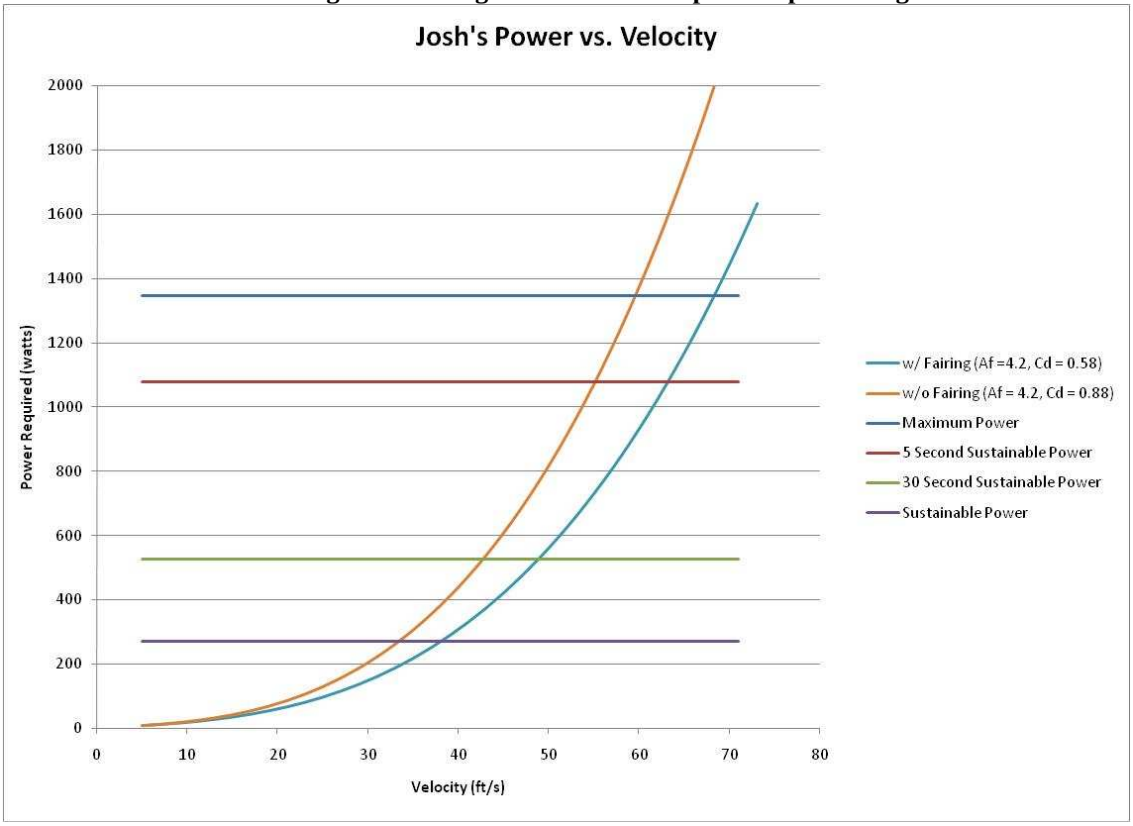

A compilation of the small, medium, and large riders' aerodynamic information and maximum velocities were compiled into Table 9. The table accounts for both losses in the drive train, and also from rolling resistance. It can be seen that through the use of the second fairing iteration, riders will gain approximately 6mph at their maximum power outputs.

Table 9. Maximum Rider Velocities

Fairing	Rider Size	Frontal Area (sq. ft.)	C_d	Max Power (Watts)	Total Drag (lbs)	Velocity (ft/s)	Velocity (mph)
Iteration 1	Anna	3.7	0.60	550	7.82	51.9	35.3
	Nick	4.0	0.60	1035	12.09	63.0	42.9
	Josh	4.2	0.62	1345	14.74	67.3	45.8
Iteration 2	Anna	3.7	0.58	550	7.74	52.5	35.8
	Nick	4.0	0.58	1035	11.96	63.8	43.4
	Josh	4.2	0.60	1345	14.59	68.0	46.3
No Fairing	Anna	3.7	0.88	550	8.85	45.8	31.2
	Nick	4.0	0.88	1035	13.71	55.7	37.9
	Josh	4.2	0.88	1345	16.54	60.0	40.9

-Motion Capture Analysis

In collaboration with the Kinesiology Department at CSUN, motion capture was conducted on two of the riders-one male and one female. The process included placing markers on specific locations along the body which are then picked up by several infrared cameras. The motion capture system used, named Equalysis, utilizes six cameras to locate each marker in almost any body position. After processing the data obtained from the cameras with the supplied software, a skeletal model was created. This was done by using the displayed markers projected on the surface of rider, where they were then identified according to the kinesiology 'plug-in gait' standard. This standard uses an algorithm, derived by the Kinesiology

Department, to locate the joints of the subject. Once the data was cleaned up and the appropriate joints identified, a skeleton was created. This allowed us to visualize the motion of the rider. Specific joint markers were then traced to see the motion pattern throughout the pedaling stroke. This analysis allowed further verification of clearance with the frame and fairing. The clearance also verified that riders would not contact any parts of the fairing during normal operation, thus ensuring a safe design. In future iterations of this design, the data could also be used in conjunction with an electromyogram, which sense muscular impulse, to further optimize geometry of foot, saddle, and handlebar position for an even more ergonomic human powered vehicle.

Figure 40. Equalysis Motion Capture of Female Rider.

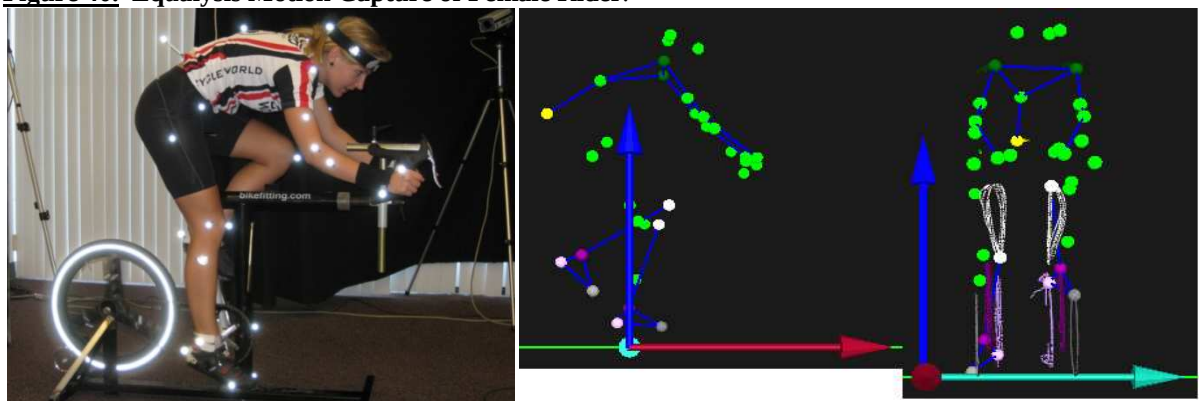

The motion capture model in Figure 40 above shows both the front and side view of the female rider. The traces of several joint markers can be seen in the image. The front knee trace shown in white is seen to be forming a teardrop shape. Ideally, the front of the knee should be moving in a vertically straight line. By using motion capture, the errors become immediately visible and can easily be corrected by properly adjusting the foot position over the pedal and height of the saddle.

Another purpose in utilizing this technology was determining the boundaries of the riders in different positions. By choosing the largest male rider and the female rider, the minimum and maximum possible body boundaries were obtained. The surface boundaries found from the initial motion capture were used to ensure the boundaries would not conflict with the riders' safety. After applying graphics software such as Maya, a more in-depth body can be created which then can be used in conjunction with Solid Works to better visualize any clearances or obstruction between the fairing, frame, and rider.

Cost Analysis

Another objective of this project was to analyze the worth of this project as a business model. The following will discuss the capital investments, parts, materials, labor, and overhead it would require to produce ten vehicles per month. This data will be used to determine the final retail prices required to support the business model and provide an acceptable profit for its investors within 3 years.

The prototype design of the P.F.C.S.U.2.W.H.P.G.V., set to unveil at the ASME 2009 West Coast Human Powered Vehicle Challenge on May 1st, 2009 is the first of its kind. Our flagship design, the P.F.C.S.U.2.W.H.P.G.V. will be featured with top level components at the competition. Initial cost for this prototype reflects the manufacturer cost without a retail margin. The flagship build will be the top tier complete bike build, and will be offered to the public for 35% profit The P.F.C.S.U.2.W.H.P.G.V. is designed to be available as a frame and fairing combination, or each separately. The pair will retail for a 40% margin, and the retail price for the frame or fairing alone will be set at a 45% margin. This margin increase is rationalized by the low overhead cost of purchased components that can be added to the higher cost HPV frame and fairing.

The following is a small scale business proposal intended to launch the Partially Faired Composite Semi Upright 2 Wheeled Human Powered Ground Vehicle (P.F.C.S.U.2.W.H.P.G.V.) frame and fairing into the free market. The estimated costs of manufacturing 10 vehicles per month are analyzed and the financial feasibility of running such a business is documented in this report.

Table 10 Cost Analysis

The process of analyzing costs for this product originates with the materials and machining costs associated with the project. Provided are the expenses for the production of one, three and finally, ten frames respectively. Upon production of ten frames, the costs are significantly reduced (30%) as a result of bulk quantity order. Below are the costs of materials required for mass production of the Partially Faired Composite Semi Upright 2 Wheeled Human Powered Ground Vehicle (P.F.C.S.U.2.W.H.P.G.V.). The initial production level of this business is 10 units per month.

MATERIALS			
	\1	\3	\10
Carbon	$800/frame	$2,400.00	$5,600.00
Aluminum	$20/frame	$60.00	$140.00
Foam (Formular 150)	?		
		TOTAL	**$5,740.00**

The carbon was purchased from CST and the aluminum from Industrial Metal Supply. Foamular 150 insulation foam was purchased from _____ .Alongside the materials, the machining costs associated with mass production are as follows.

MACHINING			
	\1	\3	\10
Foam	$600.00	$1,800.00	$12,600.00
Aluminum	$220.00	$660.00	$4,620.00
		TOTAL	**$17,220.00**

One important factor affecting the machining costs is the possibility of CNC machines being purchased for in-house machining. This would eliminate the machining costs, but add to the monthly expenditure of paying off the equipment. Nevertheless, one look at the costs of these machines and the overhead required to pay off their complete price within a year projects the favorability of picking to buy the equipment. Below are the estimated costs for purchasing the required machines from a university, which is an extremely lucrative option since these machines are used far less when compared to the other used machinery in the market.

EQUIPMENT	
Haas CNC Lathe	$25,000
Haas CNC 4 Axis mill	$25,000
Welder (Millermatic 212)	$1,925.00
TOTAL EQUIPMENT	**$51,925**

The labor and manpower required to run this production facility is approximately one worker per three frames, one machinist and one supervising engineer. In this particular business proposal, the business is assumed to be owned by the practicing engineer who shall make his or her pay from the business revenue (initial revenue of $50,000 per year). All other salaries are approximated in the Table below.

LABOR				
Wrapping time	8 hrs			
Workers	1 worker/3 frames	(3 workers)		
Machinist	1			
Supervisor	1			
	/hour	**/week**	**/month**	**/year**
Pay per worker	$18.00	$720.00	$2,880.00	$34,560.00
Total Worker Pay (3 workers)	$54.00	$2,160.00	$8,640.00	$103,680.00
Total Machinist Pay (1 Machinist)	$21.35	$854.17	$3,416.67	$41,000.00
Total Manpower cost =	**$12,056.67**			

Futhermore, the overhead expenses of running a commercial warehouse are listed below.

Overhead				
	/ sq ft	**Total sq ft**	**/month**	**/year**
Property lease	$1.50	1000	$1,500.00	$18,000.00

(Commercial/Industrial)				
Electricity			$150.00	
Gas			$50.00	
Phone			$80.00	
Insurance			$500.00	Lower Estimate (nick) - $5000/yr w/ public access; $1500/yr w/o public access
		Total	**$2,280.00**	

The total costs, on a monthly basis, are as follows

Month	**Cost**
January	$42,121.67
February	$42,121.67
March	$42,121.67
April	$42,121.67
May	$42,121.67
June	$42,121.67
July	$42,121.67
August	$42,121.67
September	$42,121.67
October	$42,121.67
November	$42,121.67
December	$42,121.67

*Updated results from the cost analysis will be presented during the unveiling at the 2009 west coast HPVC on May 1st

Performance Testing

Head Tube Tear Out

The head tube/down tube section is the most critical area since a failure of the bonding wrap can cause serious injuries to the rider. A spare head tube has been constructed following the exact specifications of the head tube to be used on the final frame. This spare head tube will be bonded and wrapped to a small mock section of the down tube for a failure test to obtain the ultimate strength of that specific joint.

The joint between the head tube and down tube is a highly critical area. Due to the nature of the design, a relatively high moment is induced by the fork at this point causing the head tube to want to tear away from the down tube. A failure here would be catastrophic for the vehicle and rider, so in order to account for this inherent weak point, a multi-stepped, conservative approach was taken.

First, with the static loading condition of the rider in the aero position (160lbf on the handlebars and 90lbf on the seat), a hand calculation was done given the length of the fork and offset to the axle. It was found that a moment of about 60lbf-ft was encountered at the bottom bearing of the head tube and 5.75lbf-ft at the top. In a shock loading scenario of 5g's, as measured by an accelerometer test due to a road irregularity, these numbers would be five times as large or 300lbf-ft and 28.75lbf-ft respectively.

Second, special care was taken in the meshing process in the Femap model to ensure an accurate and reliable result from the FEA. The nodes of the intersecting down tube were meshed directly into corresponding nodes of the pre-fabricated head tube by modifying each tetrahedron to converge at the nearest node. The results showed that with the layup schedule proposed the vehicle saw at least a safety factor of 1.57 in this area, which met the project requirements. The 5g shock load results were simulated by a constant 5g loading to keep within the scope of an undergraduate study and save time, while keeping the analysis conservative. Since a constant loading of 5g's was conservative, a result showing a factor of safety less than 1 at this joint would still signify high survivability if the constant load were converted to a shock load.

Third, and finally, a physical test will be conducted using an identical section of the vehicle to include a head tube and partial down tube. A solid steel rod has been turned to the exact interfacing dimensions of the fork and a steel structure has been fabricated to hold the partial section of the down tube. A force measuring device will be attached to the mock fork and the equivalent load for the static condition shall be applied. Then a constant load equivalent to the constant load at 5g's

shall be applied. These two tests will serve to validate the previous steps of calculation and analysis. Following this test, a test of the ultimate strength of the head tube to down tube joint will be performed. Using the force required to fail the joint, a subsequent calculation may be done to rate the top speed collision survivability of the vehicle. In other words: the fastest possible speed at which the vehicle may collide with an object of mass much larger than itself and still survive.

Tuft and Wind Tunnel Verification

In order to test the aerodynamics of our design, and therefore validate our calculations, a few simple tests will be conducted. The tests will include a verification power test around the same course as the developmental power test, and a tuft test. A tuft test consists of taping several short segments of yarn or string to the fairing and then using the fairing under real world conditions. The tuft test will provide a visualization of the flow and indicate problem spots where flow separation or turbulence exists. From these test our fairing will be evaluated and any necessary changes will be made.

Subject to time constraints and logistics, the fairing will also be tested on the vehicle frame during a tow test. The tow test will take place on a straight flat road with little wind and will consist of the vehicle, complete with fairings and rider, being towed behind an automobile at incrementally increasing speeds. In line with the tow cable will be a data logging force transducer that will measure the total drag of the vehicle at a given speed. This test will validate our aerodynamic analysis and provide real world numbers as to the true value of the total drag. Finally, after the final frame and fairings are complete the vehicle with fairing and rider in place will be tested in a low speed wind tunnel in San Diego, California. The wind tunnel data will be used as a finial validation of the aerodynamic analysis and previous testing. From the wind tunnel data an accurate prediction of the vehicles performance can be calculated.

Safety Discussion

Through countless hours of research and cycling experience, the 2008-2009 CSUN Pedal Sports team has deemed that an upright vehicle configuration provides the best combination of performance, practicality and safety. Our final design consists of a composite monocoque frame of a non-traditional design as well as partial front and rear fairings. The bike and fairing are designed around the rider such that the fairing will not jeopardize the safety or practicality of the vehicle. No part of either the front or rear fairing covers the rider's body or extremities. Therefore, the rider will be able to "dismount" from the vehicle in a traditional manner. In the case of an accident in which the rider chooses not to separate from the vehicle in the traditional manner, he or she will be partially protected from side impacts by the front and rear fairings. Due to the tall slender design of the vehicle, complete roll over will not be an issue. In addition, a roll bar would restrain the rider from a traditional bicycle dismount and could therefore create an unsafe situation for the rider. Similarly, a safety harness system would force the rider to stay attached to the vehicle during a crash and could also create an extremely dangerous situation. For these reasons, we felt that roll over protection and safety restraint systems would have hindered the overall safety of the vehicle. Furher Motion Capture Verification of rider clearance during normal operation will be presented once at the competition.

WORKS CITED

[1] Armanios, E. Fracture of Composites. Lebanon: Transtec Publications Ltd., 1996.

[2] Bhgagwan D. Agarwal, Lawrence J. Broutman, K. Chandrashekhara. Analysis and Performance of Fiber Composites. New Jersey: John Wiliey & Sons, Inc., 2006.

[3]Strong, Dr. A. Brent. Fundamentals of Composites Manufacturing: Materials, Methods, and Applications. Dearborn: Society of Manufacturing Engineers, 1989.

[4] Wilson, G. David. Bicycling Science. Massachusetts: The MIT Press, 2004

[5] Tew, G.S. Sayers, A.T. "Aerodynamics of Yawed Racing Cycle Wheels." Journal of Wind Engineering and Industrial Aerodynamics 82 (1999): 209-222.